Geophysical Journal International

Geophys. J. Int. (2024) **239,** 1133–1154
Advance Access publication 2024 September 09
GJI Seismology

https://doi.org/10.1093/gji/ggae324

Multistep procedure for estimating non-linear soil response in low seismicity areas—a case study of Lucerne, Switzerland

Paulina Janusz [1], Paolo Bergamo,[1] Luis Fabian Bonilla [2], Francesco Panzera [1,3] Daniel Roten,[4] Karina Loviknes[5] and Donat Fäh[1]

[1] *Swiss Seismological Service, Department of Earth and Planetary Sciences, ETH Zürich, Sonneggstrasse* 5, 8092 *Zürich, Switzerland.*
E-mails: paulina.janusz@sed.ethz.ch ; paolo.bergamo@sed.ethz.ch
[2] *Geotechnics, Environment, Natural Risks and Earth Sciences Department, Université Gustave Eiffel,* 14– 20 *Boulevard Newton, Cité Descartes,* 77447 *Marne-la-Vallée Cedex* 2, *France.*
Email: luis-fabian.bonilla-hidalgo@univ-eiffel.fr
[3] *Biological, Geological and Environmental Department, University of Catania, Corso Italia* 57, 95129 *Catania, Italy*
[4] *San Diego Supercomputer Center, University of California San Diego,* 9500 *Gilman Dr La Jolla, CA* 92093, *USA*
[5] *Geophysics Department, Helmholtz Centre Potsdam, GFZ German Research Centre for Geosciences, Telegrafenberg,* 14473 *Potsdam, Germany*

Accepted 2024 September 4. Received 2024 July 24; in original form 2024 March 15

SUMMARY

The impact of non-linear soil behaviour on seismic hazard in low-to-moderate seismicity areas is often neglected; however, it may become relevant for long return periods. In this study, we used fully non-linear 1-D simulations to estimate the site-specific non-linear soil response in the low seismicity area, using the city of Lucerne in Switzerland as an example. The constitutive model considers the development of pore pressure excess and requires calibration of complex soil models, including the soil dilatancy parameters. In the absence of laboratory measurements, we mainly used the cone penetration test data to estimate the model variables and perform inversion for the dilatancy parameters. Our findings, using Swiss building code-compatible input ground motions, suggest a high probability of strong non-linear behaviour and the possibility of liquefaction at high ground motion levels in the case study area. While the non-linearity observations from strong-motion recordings are not available in Lucerne, the comparison with empirical data from other sites and other methods shows similarity with our predictions. Moreover, we show that the site response modelled is largely influenced by the strong pore pressure effects produced in thin sandy water-saturated layers. In addition, we demonstrate that the variability of the results due to the input motion and the soil parameters is significant, but within reasonable bounds.

Key words: Numerical modelling; Earthquake hazards; Site effects; Wave propagation.

1 INTRODUCTION

At a high level of excitation, the soil response becomes non-linear, primarily because of the strain-dependent decrease of shear modulus and increase of damping ratio above a certain strain threshold (e.g. Beresnev & Wen 1996; Bonilla *et al.* 2005; Roten *et al.* 2009). While non-linear soil behaviour has been an important topic in the seismological community (e.g. Chandra *et al.* 2015, 2016; Guéguen *et al.* 2018; Régnier *et al.* 2018; Bonilla *et al.* 2019; Régnier 2021), it is often neglected when assessing local seismic hazard in areas of low to moderate seismicity. This is mostly because of the complex and site-specific character of non-linear soil response. While the reduction of amplification factors due to increased damping often leads to a conservative evaluation of the shaking level, the seismic hazard may remain high. The reduction of shear modulus decreases the fundamental frequency of resonance f_0 and the corresponding harmonics of the soil (Régnier *et al.* 2013); hence, the site response may become closer to the resonance frequencies for some buildings. Liquefaction poses another significant risk as soils may lose their shear strength and behave like a fluid due to a sudden increase of pore pressure under undrained conditions (Kramer 1996). Moreover, large deformations can be produced during partial recovery of the shear strength of cohesionless soils because of their dilatant nature (Bonilla *et al.* 2005).

Our case study area is the city of Lucerne in Central Switzerland (Fig. 1). This region is characterized by low to moderate seismicity (Wiemer *et al.* 2016). Nevertheless, the seismic hazard cannot be neglected as the city experienced strong earthquakes in the past (e.g. a moment magnitude M_w 5.9 earthquake in 1601, Fäh *et al.* 2011) and is located on soft deposits (e.g. Poggi *et al.* 2012) that have the potential for manifesting non-linear soil behaviour. To study non-linearity in such areas, where instrumental recordings of strong

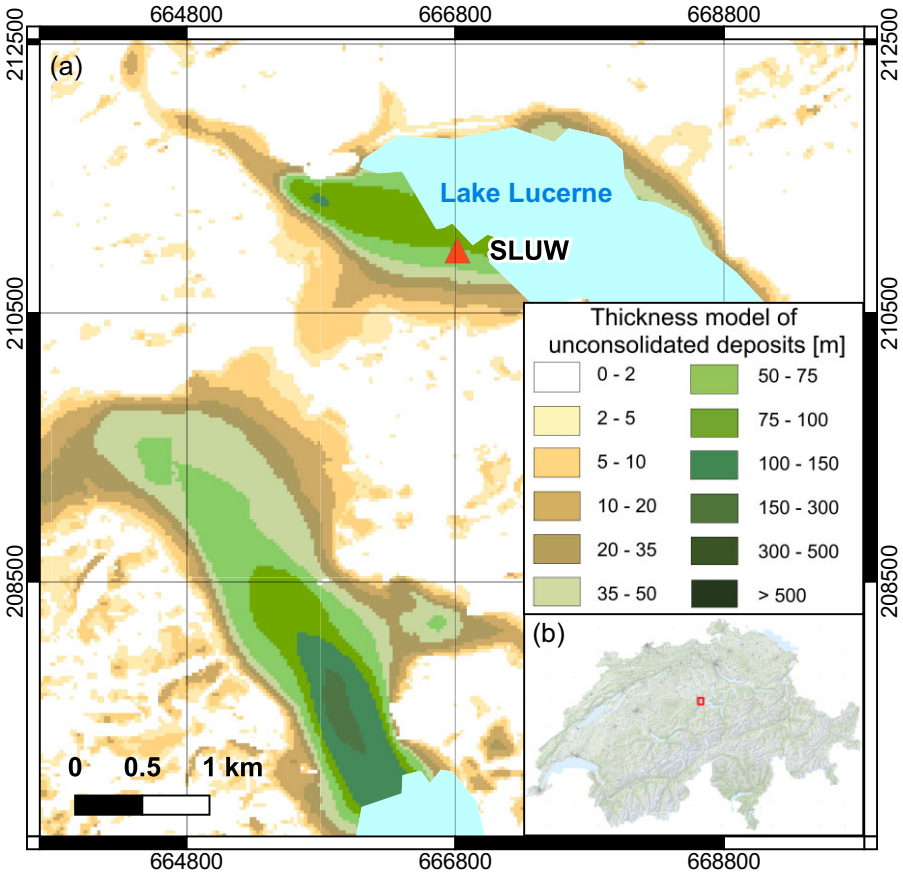

Figure 1. (a) Thickness of unconsolidated deposits in the Lucerne area (Swisstopo 2020) with marked the SLUW site (triangle). The light blue shade represents Lake Lucerne. (b) The location of the Lucerne area (red rectangle) in Switzerland. The coordinates system is CH 1903/LV03.

motion are not available, it is common to use numerical simulations either by adopting simple assumptions with a limited number of required parameters such as an equivalent linear model (Schnabel *et al.* 1972) or a more refined fully non-linear models (e.g. Yu *et al.* 1993; Yoshida & Iai 1998; Bonilla *et al.* 2005). In areas similar to Lucerne, where the groundwater table is shallow (Geoportal, Kanton Luzern 2023) and sediments are saturated, it is also important to consider the pore pressure effects and liquefaction. Many such constitutive soil models have been proposed, including, among others, plasticity-based (Elgamal *et al.* 2002), multiyield (Prevost 1985; Yang *et al.* 2003) and bounding surface models (Bardet 1986; Dafalias & Manzari 2004; Boulanger & Ziotopoulou 2015). In the framework of the VELACS project (VErification of Liquefaction Analysis by Centrifuge Studies, Popescu & Prevost 1995), a number of different constitutive models used for the numerical simulation of dynamically induced liquefaction were validated and compared, providing an extensive overview of the available models. More information can also be found in Prevost & Popescu (1996), Lade (2005) and Onyelowe *et al.* (2023). The constitutive soil model used in this work is the multishear mechanism model (Towhata & Ishihara 1985) that is implemented in the finite-difference code NOAH (Non-linear Anelastic Hysteretic, Bonilla 2001; Bonilla *et al.* 2005). It describes the hysteresis in the stress–strain relation and the pore pressure effects. NOAH uses also the liquefaction front model (Iai *et al.* 1990) that simulates the cyclic mobility and soil dilatant behaviour. Cyclic mobility in loose cohesionless soil is often referred to as liquefaction (Iai *et al.* 1990); however, the liquefaction front model does not simulate the flow failure of the soils that is typically associated with liquefaction phenomena.

For all advanced constitutive models, the calibration of necessary soil parameters remains a big challenge. One of the main advantages of the model used in this study (Towhata & Ishihara 1985; Iai *et al.* 1990) is the relatively small number of required input parameters; in addition, most of them have a physical meaning. Only a few geophysical and geotechnical parameters have to be defined for each layer (e.g. shear wave velocity V_S, density ρ, friction angle φ and cohesion c). In addition, five dilatancy parameters are needed for the liquefaction front model liquefaction (Iai *et al.* 1990). Those parameters do not have strict physical meaning in the sense of the material property; yet, they describe the geometrical development of pore water pressure under cyclic loading. Typically, the dilatancy parameters are calibrated using a laboratory triaxial test on soil samples by fitting the simulated pore pressure, strain development and the synthetic liquefaction resistance curve (LRC) to the observed data. The search can be done either using the trial-and-error method (Iai *et al.* 1990; Bonilla 2001; Bonilla *et al.* 2005; Roten *et al.* 2009), or an inversion approach (Roten *et al.* 2011). However, the availability of laboratory measurements is often low, and their cost—significant. In addition, it is sometimes questionable how well they reflect *in situ* conditions because of the use of disturbed samples (Field *et al.* 1998). Hence, some studies have attempted to invert the dilatancy parameters using strong motion from vertical array records; the simulated accelerograms using the minimum misfit models showed a

good agreement with the observations (Roten *et al.* 2014). Another solution is using the cone penetration test (CPT) data instead (Roten 2014). CPT is a popular geotechnical test, used to characterize soil geotechnical properties. An instrumented cone is pushed into the ground at a standard rate measuring sleeve friction f_s and tip resistance q_c (Liao *et al.* 2002). Some probes also have a pore pressure sensor (CPTu) or seismic piezocone modules (SCPT), allowing the estimation of the shear wave velocity profile (Liao *et al.* 2002). The CPT readings allow, among others, to estimate the soil type, its undrained shear strength and other geotechnical properties using empirical relations (e.g. Robertson & Wride 1998; NCHRP 2007; Robertson 2009a).

As soil samples and laboratory measurements were not available for the investigated area, we define the soil models for non-linear simulations based mainly on CPT data (Section 4.1), including the dilatancy parameters. They are obtained using the inversion scheme developed by Roten (2014) based on the Neighbourhood algorithm (Sambridge 1999) by inverting the LRC curve determined from CPT data (Section 4.2). This yet unpublished approach may potentially provide an alternative and cheaper approach for estimating the dilatancy parameters, compared to calibrating them using laboratory measurements. Then, we perform 1-D simulations of wave propagation in complex media (Bonilla *et al.* 2005) to estimate the impact of the non-linear soil behaviour and the possibility of cyclic mobility of the soils and liquefaction for a selected site in Lucerne (Section 4.3). However, due to the absence of strong motion data in the area to verify the results explicitly, the outcome is an indicator of non-linear soil behaviour. Yet, it can establish useful information and it is often the only source of knowledge on non-linear site response in places similar to Lucerne, even though it is only a 1-D approximation. In this paper, we explain in detail the workflow that is suitable for studying non-linear soil response (Sections 3.1–3.3) and try to assess the method's usability by investigating the impact of the associated uncertainties. We estimate the extent of the variability of the results and check if such uncertainties are acceptable. We hypothesise that the variability of the input ground motions and the uncertainty of the soil parameters from CPT data, including dilatancy parameters, have the highest impact on the method's epistemic uncertainty. Therefore, we investigate the sensitivity of the results using different input ground motions (Section 4.4), a wide range of dilatancy parameters (Section 4.5), and several soil models with varying parameters (Section 4.6). We treat the dilatancy parameters separately as the inversion procedure produces a range of feasible results (Roten 2014; Janusz *et al.* 2022a) and we want to understand their impact. Finally, we compare the results to empirical observations of soil non-linearity in other sites (Section 5.1) and results from other methods (Section 5.2) to assess if our findings lie within a similar range of values. Based on the results, we discuss the drawbacks of the sensitivity analysis, and the usability and the advantages of the method proposed (Section 5.3). The paper aims to present the workflow that allows estimating the non-linear site response using *in situ* geotechnical data; and which is applicable in a wide range of settings, in particular in the low seismicity urban areas.

2 GEOLOGICAL SETTING, HISTORICAL SEISMICITY AND DATA

Lucerne is the 7th biggest most populated city in Switzerland (about 80 000 inhabitants, Bundesamt für Statistik 2023) and population density of about 2200 people km^{-2}. Although it is located in an area with a low seismicity level in the period of modern instrumental observation, strong earthquakes occurred in the past (Gisler *et al.* 2004). Several strong earthquakes are known from historical and geological records, including, among others, the event in 1601 with an M_w of 5.9 (Fäh *et al.* 2011) and three palaeoevents with an estimated M_w of 6.5–7.0 (Strasser *et al.* 2006; Kremer *et al.* 2020). Earthquake Catalogue of Switzerland 2009 (ECOS-09, Fäh *et al.* 2011) provides the full list of the historical and recorded seismic events in the area. The local seismic hazard at the rock reference is low-to-moderate according to the Seismic Hazard Model for Switzerland 2015 (SUIhaz15, Wiemer *et al.* 2016), while the seismic risk is relatively high due to the strong soil amplification and vulnerability of the buildings, placing the city 4th in the ranking of Swiss cities with the highest seismic risk (Earthquake Risk Model of Switzerland ERM-CH23, Papadopoulos *et al.* 2023; Wiemer *et al.* 2023). There is no published evidence of past non-linear soil behaviour or occurrence of liquefaction in the city; however, strong deformations and sediment-slope failures that suggest liquefaction were found in the nearby lake sediments (Siegenthaler *et al.* 1987; Schnellmann *et al.* 2002). Moreover, the city is located in a basin filled with soft, saturated, fluvial-lacustrine sediments (mostly sand, gravel, clay and silt) that are prone to strong site effects and potential liquefaction (e.g. Poggi *et al.* 2012; Resonance & Keller and Lorenz AG 2012).

The study site (Fig. 1) is located in the Lucerne city centre close to the lakefront in the relatively thick part of the sedimentary basin (about 70 m of deposits, Swisstopo 2020). The sediments are classified as artificial filling (Swisstopo 2023) and are assigned to soil class D by the Swiss national soil class map (Keller & Lorenz AG 2010; Mayoraz *et al.* 2016). Such soil class is characterized by a time-averaged shear wave velocity to a depth of 30 m (V_{S30}) of less than 300 m s^{-1}. The site shows a f_0 at about 1.2 Hz and the expected amplification factors are more than ten at about 1.2 Hz and remain high (>5) at higher frequencies (Edwards *et al.* 2013; Janusz *et al.* 2022c). The site was chosen due to the large number of geophysical measurements performed nearby as a part of site characterization of the permanent seismic station SLUW of the Swiss Strong Motion Network (SSMNet, SED 1983; Cauzzi & Clinton 2013; Poggi *et al.* 2013; Diehl *et al.* 2014; Michel *et al.* 2014; Hobiger *et al.* 2021). The geophysical and geotechnical data available include active and passive seismic measurements, CPT and SCPT (Poggi *et al.* 2012, 2013; SED 2015).

3 METHODOLOGY AND PROCESSING

The workflow we propose (Fig. 2) consists of three main steps: (a) calibration of the soil model, (b) inversion for the dilatancy parameters for layers that are prone to liquefaction and (c) simulation of wave propagation in the non-linear media.

3.1 Soil model definition

We define a 1-D soil model for the SLUW site, assuming that the uppermost layers are non-linear (above 30 m depth, which is the maximum depth of the CPT survey at the site). The deeper part of the profile is considered linear viscoelastic (up to the bedrock depth) as the significant non-linear soil behaviour occurs mostly in shallow sediments (Régnier 2013). The constitutive model for non-linear layers, which is based on the multishear mechanism and liquefaction front model (Towhata & Ishihara 1985; Iai *et al.* 1990), requires specifying several parameters that are listed in Table 1. For

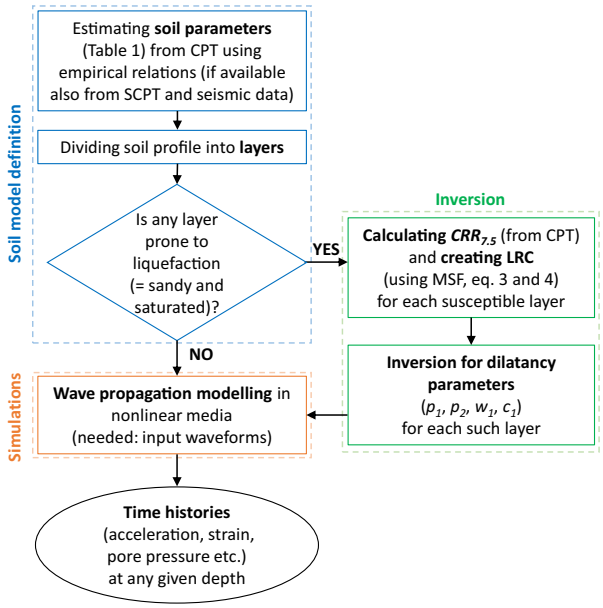

Figure 2. The flowchart illustrating the main steps of the procedure.

linear viscoelastic layers, it is required to specify V_S, ρ and quality factor Q.

We use CPT and SCPT data to assign the parameters for the shallow part of the soil profile (surficial 30 m). As there are several empirical equations described in the literature (Table 1) that allow deriving geotechnical and geophysical parameters from CPT, we define a soil model for the SLUW site by calculating the mean over several equations to reduce subjectivity (bolded relation in Table 1). The CPT data and their interpretation are plotted in Fig. A1 in Appendix A. For V_S, we choose the SCPT (Fig. 3a) as it is a direct measurement. For deriving shear wave velocity from SCPT, we use a damped least square inversion method (Hobiger *et al.* 2021). We divide the profile into layers and for each; we attribute the mean value of a given parameter, creating a reference model for the SLUW site (values in Table A1 in Appendix A). We identify sandy-silty layers in the model based on lithological interpretation from CPT using soil behaviour type index (I_c, Robertson & Wride 1998; Fig. 3b).

In addition, to study the sensitivity of the shallow part of the profile, we create several other soil models, either by randomly selecting one equation from Table 1 for each parameter independently (100 combinations) or by changing only one parameter and keeping the reference model for the rest (25 combinations in total, i.e. eight models where V_S profiles vary, eight with different ρ, etc.). As some parameters are connected (e.g. coefficient of the Earth pressure at rest K_0 is calculated from friction angle φ), changing one parameter requires recalculations of the whole profile to avoid non-physical models. The water table depth is specified to be 0.5 m based on the groundwater map (Geoportal, Kanton Luzern 2023). As the site is located very close to the lakeshore, typically a stable surficial water table level is retained with not much variation. The yearly variations are lower than 0.5 m for the closest measurement location (about 700 m away). For the sensitivity analysis, we test values between 0–2 m depths of the groundwater table (Table 1). To define the shear-wave velocity profile (Fig. 3c) for the deeper part of the soil profile (below 30 m up to bedrock depth), we use the active and passive surface wave measurements (Poggi *et al.* 2013). They are inverted using the dinver algorithm from the Geopsy package (Wathelet *et al.* 2004) adopting geological constraints for the bedrock depth (about 70 m, Swisstopo 2020).

3.2 Inversion for dilatancy parameters

For layers susceptible to cyclic mobility and liquefaction (i.e. sandy-silty water-saturated layers), we need to define five dilatancy parameters that describe the pore pressure excess development in the liquefaction front model (Iai *et al.* 1990). The model was developed based on the observation of the correlation between the excess pore pressure and the cumulative shear work produced during cyclic loading (Towhata & Ishihara 1985). The dilatancy parameters control the shape of the function of the pore pressure evolution in time. Initial dilatancy p_1 controls how fast the pore pressure rises during the initial phase of deformation (Fig. 4), while final dilatancy p_2– in the terminal phase. Overall dilatancy w_1 describes the general shape of the curve. The lower p_1 and w_1, the faster the pore pressure increases, while low p_2 means a slower rise. The threshold limit c_1 shows the threshold limit of the shear work when the pore pressure build-up starts. The state parameter S is a function of the cumulative shear work w (Iai *et al.* 1990):

$$S = 1 - 0.6\left(\frac{w}{w_1}\right)^{p_1}, \; if \; w < w_1 \tag{1}$$

$$S = (0.4 - S_1)\left(\frac{w}{w_1}\right)^{p_2} + S_1, \; if \; w > w_1 \tag{2}$$

As S cannot be zero for numerical stability, the parameter S_1 with a small positive value (0.01) is introduced to prevent it. S equals one means that there is no pore pressure excess generated, while S approaching zero says that the effective confining stress is close to pore water pressure. It indicates that the soil is on the verge of completely losing its shear strength and liquefying.

We estimate the dilatancy parameters following the inversion procedure of Roten (2014) that was tested using synthetic examples (Janusz *et al.* 2022a, b). The first step of the method is to estimate the cyclic resistance ratio $CRR_{7.5}$ from CPT (Robertson & Wride 1998; Robertson 2009b). The $CRR_{7.5}$ is defined as the cyclic stress ratio (CSR) required for triggering liquefaction during 15 uniform loading cycles that are assumed to correspond to a magnitude 7.5 earthquake. If the CSR is high, only a few cycles are required to trigger liquefaction, while for low CSR, many cycles, which correspond to strong and long-duration earthquakes, are necessary. The relation of the CSR and the number of cycles (N) to liquefaction is the liquefaction resistance curve (LRC, Fig. 5) that is derived from $CRR_{7.5}$ using magnitude scaling factors (MSF, Idriss & Boulanger 2006):

$$CSR = CRR_{7.5} \cdot MSF \tag{3}$$

$$N = \frac{15}{MSF^{\frac{1}{0.337}}} \tag{4}$$

In this study, the LRC curve is constructed using 14 MSF values evenly distributed between 0.4 and 1.8.

We then invert, based on the Neighbourhood algorithm (Sambridge 1999), the set of four dilatancy parameters (p_1, p_2, w_1 and c_1) that can reproduce the LRC. Contrary to the typical trial and error method (Iai *et al.* 1990), where individual dilatancy parameters are determined sequentially at different shear stress levels, here they are jointly estimated. The model space limits for a search are

Table 1. Required soil model parameters that are estimated using empirical relations from CPT, direct measurements (SCPT), or assumed. The versions used for the creation of the SLUW reference soil model are in bold; the values are given and plotted in Appendix A.

Parameter	Soil rheology	Empirical relation/Value
Shear wave velocity (V_S) [m s^{-1}]	Linear	1–Hegazy & Mayne (1995)–eq. 6
	Non-linear (effective and total)	2–NCHRP (2007)—eq. 11
		3–Hegazy & Mayne (2006)—eq.6
		4–Robertson (2012)—eq. 28
		5–mean over 1–4
		6–SCPT
		7, 8–SCPT ± standard deviation
Density (ρ) [kg m^{-3}]	Linear	1–Robertson & Cabal (2010)—eq.2
	Non-linear (effective and total)	2–Mayne (2014)—eq.2a
		3–Mayne (2014)—eq.2b
		4–NCHRP (2007)—eq. from fig. 31
		5–mean over 1–4
		6–Nagashima & Kawase (2021)—eq.10
		7–Nagashima & Kawase (2021)—eq.11
		8–Héloïse *et al.* (2012)—p.434
Quality factor (Q) [–]	Linear	**1–Olsen (2000)—p.S80**
	Non-linear (effective and total)	2–Brocher (2007)—eq.5
		3–Poggi & Fäh (2015)—eq. 3.2
Coefficient of the Earth pressure at rest (K_0) [–]	Non-linear (effective and total)	**1–Mayne & Kulhawy (1983)—eq.10**
		2–$K_0 = 0.5$ (normally consolidated)
		3–$K_0 = 1$ (isotropic)
Friction angle (φ) [°]	Non-linear (effective and total)	1–Kulhawy & Mayne (1990)—eq. from fig. 4–17
		2–Kulhawy & Mayne (1990)–eq. 4–12
		3–mean over 1–2
Depth of the water table [m]	Non-linear (effective and total)	1–0.0
		2–0.5
		3–1.0
		4–2.0
Cohesion (c) [Pa]	Non-linear (effective and total)	**1–Mesri & Abdel-Ghaffar (1993)—eq. from fig. 4 and NCHRP (2007)—eq. 26**
		2–Mesri & Abdel-Ghaffar (1993)—eq. from fig. 4 and NCHRP (2007)—eq. 19
		(sandy layers are assumed cohesionless)
Phase transformation angle [°]	Non-linear (effective)	Ishihara & Towhata (1982)
Porosity (Φ) [–]	Non-linear (effective)	0.45 (assumed)
Dilatancy parameters	Non-linear (effective)	see section 3.2

given in Table 2 and are based on the definition of the dilatancy parameters in the constitutive model (Iai *et al.* 1990) and the performed tests of the inversion procedure (Janusz *et al.* 2022a, b) that showed that the model space must be constrained by using the ranges from literature (Iai *et al.* 1990) to obtain realistic values of the dilatancy parameters. Several parameters control the sampling of the model space in the Neighbourhood algorithm (Table 3). In the initial phase of the inversion, the model space is divided into ns_0 cells (sample size for the first iteration). Then, each of the nr cells (the number of cells to resample) with the lowest misfit is divided into ns/nr new cells where ns is the sample size for all other iterations. The process is repeated until $n_{\max}$ (maximum number of iterations) is achieved. The results of the inversion for the dilatancy parameters are often non-unique, hence, the algorithm needs to be explorative to find different local minima, but at the same time, it has to be time-effective. Table 3 shows the parameters that were chosen based on the initial tests of the inversion procedure (Janusz *et al.* 2022a, b) that allow the adequate search of the model space.

As a forward model in the inversion, we simulate the stress-controlled experiment (Fig. 4) for each CSR value (Fig. 5) in simple shear mode using the liquefaction front model (Iai *et al.* 1990). The applied stress σ_{xy} in the experiment is a function of the number of cycles N, CSR and mean effective stress σ'_0, while d_t is a time step:

$$\sigma_{xy} = \sin\left[2.0 \cdot \pi \cdot d_t \cdot (N-1)\right] \cdot CSR \cdot \sigma'_0 \tag{5}$$

We look for the models where liquefaction is triggered for similar CSR values and number of cycles as in the LRC curve (Fig. 5). It is assumed that liquefaction starts when the strain reaches 2.5 per cent (5 per cent double amplitude). The misfit between the model and empirical data is calculated as in eq. (6), where n is the number of samples in the LRC curve (Fig. 5):

$$misfit = \sum_{k=1}^{n} \left(\frac{data_k - model_k}{model_k} \right)^2 \tag{6}$$

For low CSR values, the 2.5 per cent strain may not be reached within a specified time because the stresses are too low; the adopted solution in such cases is to remove the lowest values of the CSR.

3.3 1-D wave propagation in non-linear media

We simulate wave propagation in water-saturated non-linear media with vertically incident horizontally polarised shear (SH) waves using the 1-D finite-difference code NOAH (Bonilla 2001; Bonilla *et al.* 2005). The code can model linear viscoelastic and non-linear

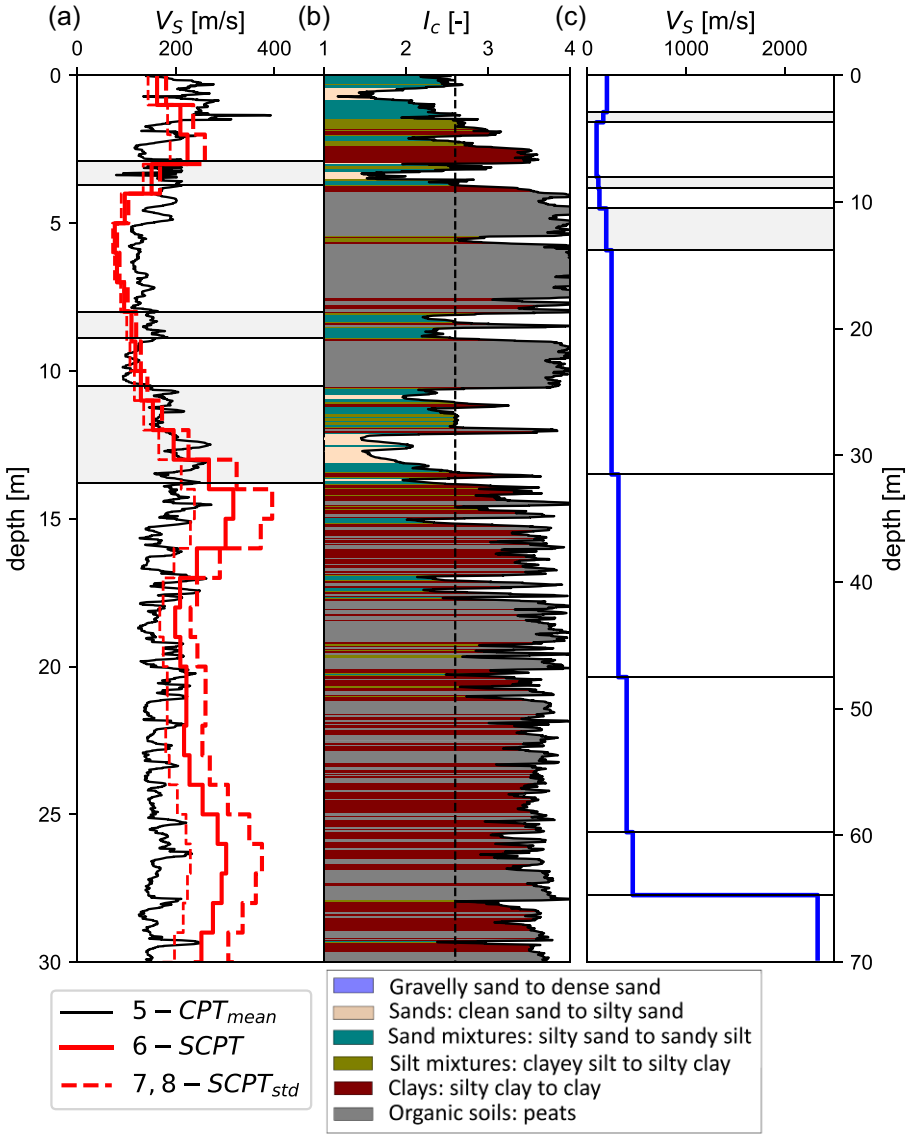

Figure 3. (a) Shear-wave velocity profiles using selected interpretations of CPT and SCPT (Table 1) for the first 30 m of the profile. The layering of the SLUW reference soil model is shown using horizontal lines; sandy liquefaction-prone layers are marked using grey rectangles. (b) Lithology interpreted from CPT using soil behaviour type index (I_c, Robertson & Wride 1998) for the first 30 m. (c) Shear-wave velocity profile for the SLUW site up to the bedrock depth.

media performing simulations without (total stress), and with (effective stress) generation of excess pore water pressure. For effective stress, the code implements the liquefaction front model (Iai *et al.* 1990) that simulates the cyclic mobility of dilatant sands under undrained conditions. In all non-linear layers, hysteretic damping following extended Masing rules (Masing 1926) is used. Intrinsic attenuation, or small-strain damping, follows the generalised Maxwell body rheology, assuming a frequency-independent quality factor Q (Day 1998) for all layers—whether they are viscoelastic or non-linear. Only the sandy-silty water-saturated granular layers in the soil models are supposed to produce pore pressure effects; an effective stress analysis is performed. Other non-linear layers use the total stress condition where the generation of pore pressure excess is not computed. However, the water table is considered to calculate the effective vertical stress for all saturated layers even in the case of total stress analysis (Bonilla 2001). Finally, the deep part of the soil profile (depth $>$ 30 m) is assumed linear viscoelastic. The input parameters for NOAH are given in Table A2.

We simulate the soil response using input ground motions applied at the bedrock depth. As for the input ground motions, we use design-compatible waveforms that were selected by Panzera *et al.* (2023a, b, 2024) as a part of the project that aimed to provide a database of the input motions suitable for microzonation studies in Switzerland. The waveforms are consistent with the normative elastic response spectra for soil class A (i.e. outcropping rock with V_{S30} $>$ 800 m s^{-1}) according to the Swiss building code (SIA261 2020). The normative elastic response spectra (SIA261 2020) are related to the values of the Uniform Hazard Spectra (UHS) of SUIhaz15 which is referred to the outcropping rock reference (Poggi *et al.* 2011). As the used input ground motions are recorded at the surface, we divide them by 2 to account for the free surface effect and use the elastic boundary at the base of the soil column. The procedure of selecting the waveforms which is described in detail in Panzera *et al.* (2023a, b, 2024) uses the Baker & Lee (2018) algorithm that is adapted to implement the compatibility criteria listed in the draft of Eurocode 8 (2023). In particular, it was ensured that at each period of a vector

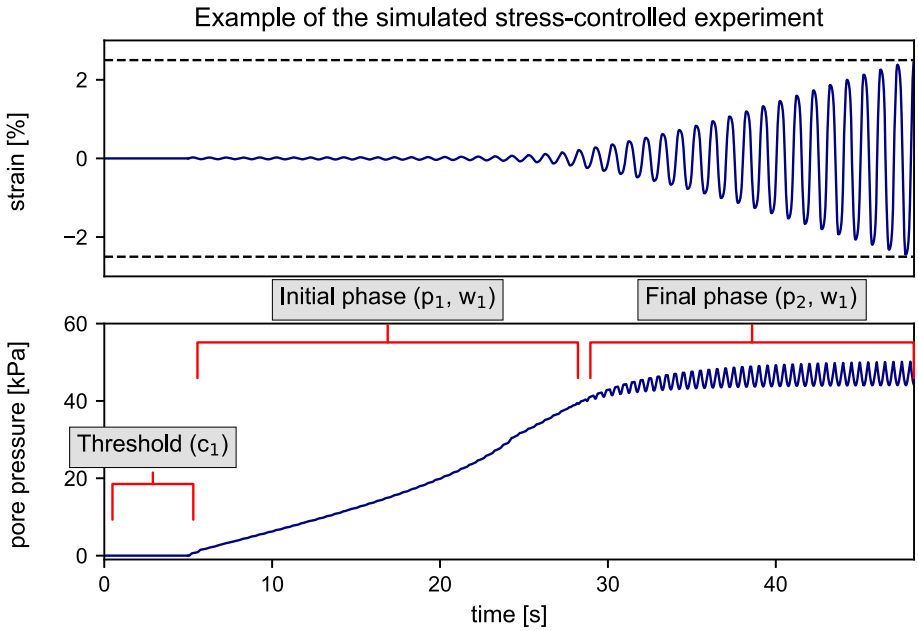

Figure 4. Strain and pore pressure development in one example of the simulated stress-controlled experiment that was performed for the middle sandy layer at the depth of 8.45 m (layer no. 5 in Appendix A) with a CSR value of 0.07. The areas of effect of individual dilatancy parameters are shown; however, the influence of c_1 was exaggerated for visualisation purposes by moving the resulting curves to the right.

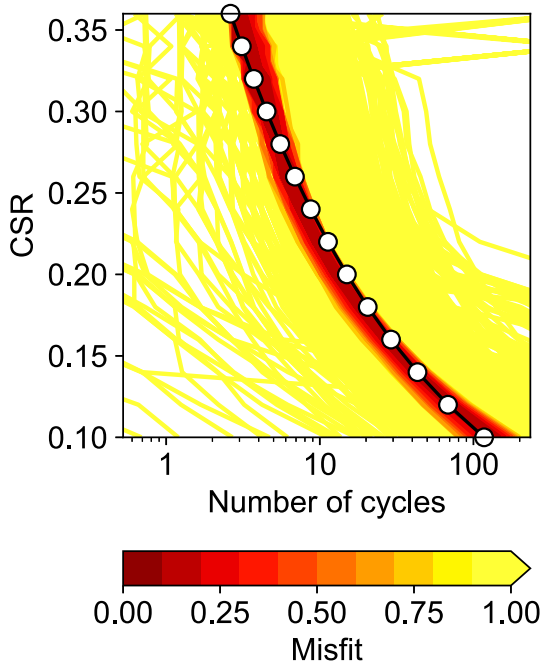

Figure 5. LRC curve (in black with white markers) from CPT for the sandy layer at the depth of 12.15 m (layer no. 7 in Appendix A) compared to LRCs generated during one run of inversion with misfit indicated by colour.

of 30 logarithmically spaced samples between 0.02 and 2 s, the ratio between the mean of the 5 per cent-damped response spectra of the waveform set and the target spectrum fell within the range 0.75–1.3 (Fig. B1 in Appendix B). Additionally, the average ratio across the entire period range was constrained to be ≥95 per cent, and every accelerogram in the set exceeded 50 per cent of the target spectrum

Table 2. Location of the silty-sandy layers in the SLUW reference soil model and the lowest misfit set of dilatancy parameters. In addition, the model space search ranges for the inversion are given. Layer 1 is the deepest layer and Layer 3 is the shallowest.

	Layer 1	Layer 2	Layer 3	Search range
p_1	1.00	0.90	0.99	0.4–1.0
p_2	1.87	0.84	1.78	0.6–2.0
w_1	7.65	1.52	6.41	0.0–20.0
c_1	1.00	0.59	0.93	0.0–2.5
Mid-depth [m]	12.15	8.45	3.3	
Thickness [m]	3.3	0.9	0.8	

Table 3. Parameters used in this study for the Neighbourhood algorithm (Sambridge 1999).

Parameter	Value
n_{max}	500
ns_0	128
ns	128
nr	64

at any period. The applied scaling factors did not exceed the range of 0.5–2.

It was demonstrated that 11 waveforms are sufficient for the site response studies (Perron *et al.* 2022); hence, we use a set of 11 waveforms that are compatible with the importance of class III structures (e.g. bridges, hospitals), which corresponds to spectral accelerations expected for a return period of about 975 yr (Table 4). In the Swiss building code, the spatial variability of the hazard in Switzerland is modelled using five seismic zones (SIA261 2020)—it was ensured by Panzera *et al.* (2023a; b, 2024) that the selected waveforms are as compatible as possible with the seismic hazard for a given seismic zone, indicating a range where the magnitude–distance pairs should lie based on disaggregation (Bergamo *et al.* 2021, 2022) of SUIhaz15. For the set of waveforms selected (Table 4), we use the

Table 4. Metadata of 11 scaled waveforms for seismic zone Z2 (SIA261 2020) and a return period of about 975 yr. The initial PGA values before scaling are given. The waveform sources are the European Strong Motion Database (ESM, Luzi *et al.* 2016), the K-NET and KiK-net databases (Aoi *et al.* 2011) and the Pacific Earthquake Engineering Research Center (PEER NGA WEST 2, Ancheta *et al.* 2014). The abbreviation *Rjb* refers to Joyner-Boore distance.

No.	M_w	*Rjb* [km]	Date	Time	Duration [s]	PGA [m s^{-2}]	Scale factor	V_{S30} [m s^{-1}]	Database
1	5.2	1.6	25.10.12	23:05:24	3.0	1.82	1.18	1906	ESM
2	6.6	17.2	06.10.00	13:30:00	17.0	1.81	1.29	929	K-NET & KiK-net
3	6.6	78.2	20.03.05	10:53:00	20.4	0.80	1.93	1002	K-NET & KiK-net
4	5.9	10.4	26.10.16	19:18:06	7.7	1.67	1.13	>800	ESM
5	5.9	6.8	26.10.16	19:18:06	7.3	0.84	1.69	>800	ESM
6	6.5	9.8	30.10.16	06:40:18	12.7	1.90	0.67	>800	ESM
7	6.5	32.9	30.10.16	06:40:18	13.9	0.81	1.75	>800	ESM
8	5.6	49.4	13.12.90	00:24:26	19.8	0.89	1.78	>800	ESM
9	5.2	9.6	25.10.12	23:05:24	4.6	1.17	1.89	>800	ESM
10	6.7	15.1	17.01.94	12:31:00	6.6	1.56	0.82	1223	PEER NGA WEST 2
11	6.1	23.1	14.04.16	21:26:00	11.3	1.66	1.42	765	K-NET & KiK-net

waveforms prescribed for zone Z2. Although Lucerne is located at the border of seismic zones Z1b and Z2, we choose the more conservative zone Z2, because we want to observe cyclic mobility and the onset of the liquefaction and weaker input motions may not trigger them.

As mentioned, we use the set of 11 waveforms (Table 4), corresponding to the local seismic hazard for a return period of about 975 yr for zone Z2. In our analysis, we also want to show the dependence of the results on the peak ground acceleration (PGA) of the input waveform. However, the 11 waveforms selected (Table 4) cover only a very limited range of PGA values (between 1.27 and 2.36 m s^{-2}). Hence, to show the dependence on PGA, we also include waveforms with different levels of hazard (475 yr return period—structure importance class I, e.g. residential buildings), and for a zone Z1b, extending the PGA range down to 0.53 m s^{-2} (the list of all waveforms used is shown in Appendix B). We also scaled the amplitudes of some waveforms by a scalar value to cover an even broader range of PGA (down to 0.005 m s^{-2}). We calculate spectral ratios between soil surface and bedrock, which can be equated to surface-to-borehole spectral ratios (SBSR). The Fourier amplitude spectra for SBSR computations are smoothed using Konno & Ohmachi (1998) algorithm with a *b*-value of 40. To assess the effects of the non-linearity at the surface, we compare the results to the viscoelastic SH transfer function (SHTF) calculated using the code TREMOR. It computes the transfer function in a layered, damped soil on an elastic rock in the frequency domain. In the code, a frequency-independent Q model is implemented (Kjartansson 1979). Following Régnier *et al.* (2013) and Loviknes *et al.* (2022), we calculate the amplitude change index (ACI) and shift of frequency (S_h) between linear and non-linear SBSRs to quantify the degree of non-linearity. Additionally, for each waveform, we compute the significant duration defined as the time interval between 5 and 95 per cent (Trifunac & Brady 1975) of Arias intensity (Arias 1970).

4 RESULTS

4.1 Soil model

We create the reference soil model for the SLUW site using CPT, SCPT, and seismic data as explained in Section 3.1. It consists of 11 layers, including eight units where we consider non-linear effects and three water-saturated sandy-silty layers prone to liquefaction (Table 2). The values for each layer are given in Table A1 in Appendix A.

According to CPT interpretation, thin intermixed layers of sand, silts, clays and organic soils are present in the first 15 m of the soil profile (Fig. 3b); the *S*-wave velocity profiles estimated from SCPT and empirical relationships based on CPT (Table 1) are fairly similar until that depth (Fig. 3a). Below, where clays and organic soils dominate (Fig. 3b), the V_S from CPT is slightly lower (Fig. 3a). However, the differences are not significant and the velocity profile derived from CPT can be still used as an acceptable approximation. The S-wave velocity of the deeper part of the profile (Fig. 3c) does not exceed 500 m s^{-1} down to the bedrock, which is estimated to be at about 65 m depth with $V_S \sim 2300$ m s^{-1}. We compare the calculated viscoelastic SH transfer function (SHTF), corrected to the free surface of the Swiss standard rock profile (Poggi *et al.* 2011), and the observed empirical amplification functions (EAF) for the seismic station SLUW, obtained with empirical spectral modelling (Edwards *et al.* 2013). They agree in terms of f_0 and, to some extent, amplitude (Fig. 6). Even though it is not an excellent fit, especially at higher frequencies, our soil model is a sufficient approximation and it can explain the empirical amplification to some degree, which is crucial because the non-linearity is defined with respect to linear site response. The reason for the discrepancies may be the fact that the linear response at the SLUW site might also be affected by 2-D and 3-D site effects and edge-generated surface waves (Poggi *et al.* 2012, 2013), as it is located in a sedimentary basin. Based on available geological information (Fig.1), the Lucerne basin should not fulfil the existence conditions criteria for 2-D resonance according to Bard & Bouchon (1985), but it is likely to host lateral propagations (edge-generated surface waves).

4.2 Inversion of dilatancy parameters

We perform the inversion for the dilatancy parameters for three sandy layers in the SLUW reference soil model, following the procedure described in Section 3.2. The red dots in Fig. 7 show the sets of inverted dilatancy parameters for the middle sandy layer (about 8.45 m depth). The best set, in terms of misfit, is marked with a red line (Fig. 7, Table 2). The results for c_1 and w_1 are quite consistent within the investigated model space, converging to one value. On the other hand, p_1 and p_2 show several minima and dispersed results,

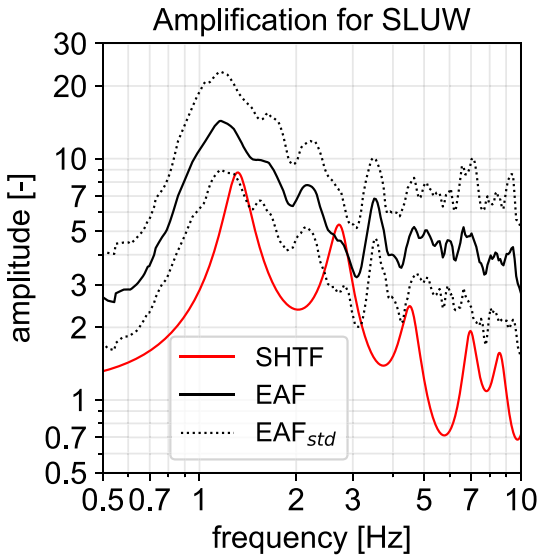

Figure 6. Comparison of the EAF and SHTF for the SLUW reference soil model. Both amplification curves are referenced to the Swiss standard rock velocity profile (Poggi *et al.* 2011).

indicating the non-uniqueness of the considered inverse problem. For the deepest and shallowest sandy layers (Appendix C), c_1 and w_1 are also consistent, while the values of p_1 and p_2 tend towards the maximum limit of the search range. Some preliminary tests on the influence of the soil model have already been performed (Janusz *et al.* 2022a). In this study, we systematically investigate its impact by running inversions for 25 different soil models that use different empirical equations from Table 1 changing one relation at a time. The variability in Fig. 7 (black dots) is much higher but shows similar trends to the inversion of the SLUW reference model (i.e. p_1 and p_2 values show a large spread while c_1 and w_1 are quite consistent). Although we have not tested all possible combinations of the soil parameters, such a basic sensitivity analysis provides a sufficient overview of the behaviour of the inversion for a specific soil layer. It also allows testing the impact of that variability on the ground motion simulation (see Section 4.5).

4.3 Non-linearity and liquefaction in 1-D wave propagation simulations

We simulate the 1-D wave propagation at the SLUW site using the finite-difference code NOAH for the 11 horizontal-component waveforms from Table 4 (compatible with the local hazard for about 975 yr return period), as described in Section 3.3. We observe strong non-linearity—Fig. 8 shows an example of an accelerogram simulated at the surface compared to the respective linear viscoelastic case. We see typical signs of non-linearity with diminished amplitudes and reduced high-frequency content. The SBSRs in Fig. 9 for non-linear simulations considering pore pressure excess generation (effective) or disregarding it (total stress analysis) for granular layers are compared to the linear viscoelastic site response. Non-linear calculations show the shift of the f_0 towards lower frequencies and strong damping and de-amplification of the ground motion, especially at high frequencies (>5 Hz).

As the simulations using total stress analysis show less non-linearity in terms of reduction of wave amplitudes and change of f_0 (Fig. 9), we investigate the variation of PGA and maximum shear strain along the profile (Fig. 10). Differences are mainly seen in the middle sandy layer. For the effective stress analysis, the mean PGA for that layer is almost 20 m s^{-2} and the simulated strain is 2–3 per cent, showing strong deformations. This indicates significant cyclic mobility of the dilatant soil and possible liquefaction. The values are larger than those from total stress analysis, in which the development of pore pressure excess is not modelled. However, the average PGA at the surface is very similar for both effective (1.1 m s^{-2}) and total stress analysis (1.3 m s^{-2}) and at the same time, much lower than for linear viscoelastic model (4.5 m s^{-2}). Hence, using only the PGA

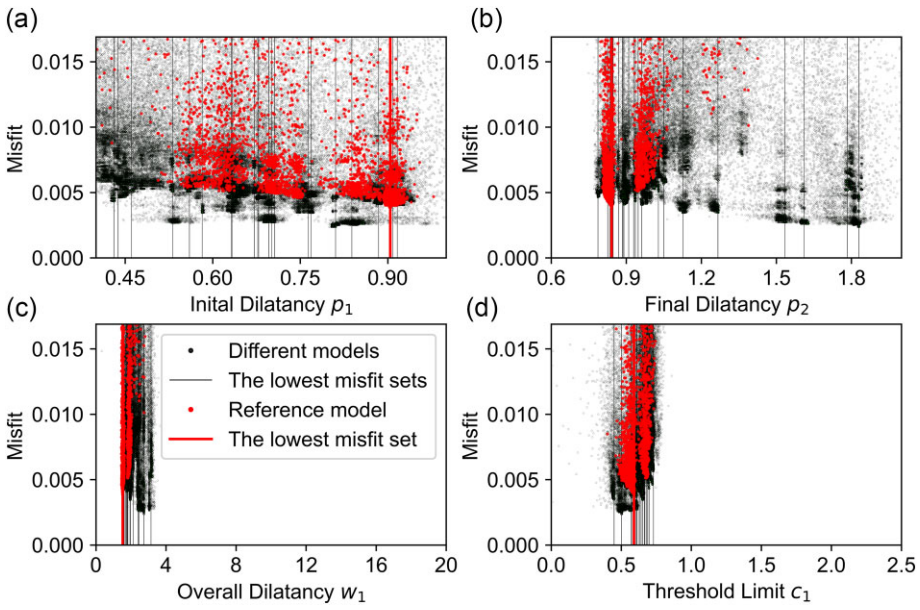

Figure 7. Misfit of the inverted sets of dilatancy parameters for the middle sandy layer. The lowest misfit set is shown as a vertical line. Red dots and the red line indicate the results for the reference model for the SLUW site, and black dots and black lines the results for 25 modified models. The *x*-scale limits represent the model search ranges for each dilatancy parameter (Table 2).

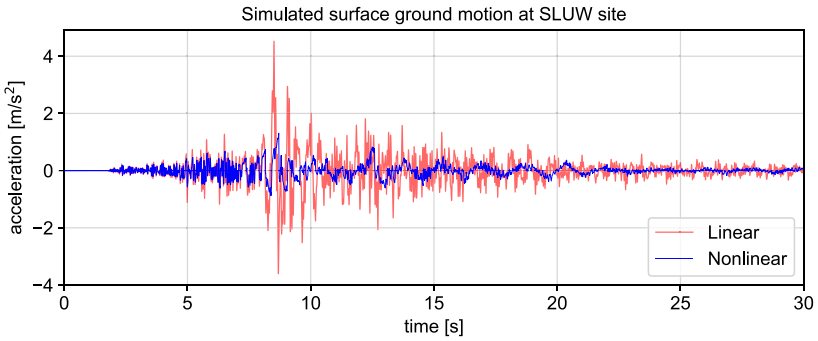

Figure 8. Comparison of the surface ground motion at the SLUW site simulated using linear viscoelastic and non-linear rheology for waveform no. 2 (Table 4).

value at the surface, we cannot distinguish if the strong dilatant effects in the soils occurred.

For each of the 11 waveforms from Table 4 (one example in Fig. 11), we observe strong hysteretic behaviour of stress–strain relation at the depth of 8.45 m in the middle sandy layer, while the stress-confining pressure plot shows typical soil dilatant behaviour (Bonilla *et al.* 2005; Roten *et al.* 2009). Moreover, the state parameter S is close to zero, indicating that the soil is on the verge of liquefaction. In all examples, we first see a strong acceleration peak at the considered depth while pore pressure suddenly increases, which is then followed by strong cyclic mobility (S approaching zero) and high strain, especially in the first phase of deformation. Such behaviour (i.e. high acceleration peak and strong initial deformation phase) indicates significant mobilisation of the soil.

We extend the analysis to the larger set of input ground motions (covering a broader range of PGA levels) by using all waveforms listed in Appendix B. Strong pore pressure effects affect the middle sandy layer for many waveforms (Fig. 12). For PGA at the surface between 0.6 and 1.0 m s^{-2}, the middle layer shows strong dilatant behaviour and the possibility of liquefaction for some waveforms, while above 1.0 m s^{-2}—the large pore pressure effects become inevitable. The PGA threshold of liquefaction is consistent with values reported in the literature, that is 0.7–1.0 m s^{-2} (Santucci de Magistris *et al.* 2014). For two other sandy-saturated layers, cyclic mobility does not occur or is observed for a very limited number of ground motions. Generally, strong pore pressure effects are correlated with the high values of PGA in the layer and extensive strain (Figs D1 and D2). We observe a clear correlation of the state parameter S with the PGA of the input waveforms (Fig. D3), showing a link between strong pore pressure effects and the intensity of the input ground motion. We have also expected that the durations of the input motions might play a role, as with an increasing number of cycles, the cyclic resistance of the soil decreases. Indeed, we observe some correlation using 11 waveforms from Table 4 (Fig. D4) but only for the middle layer, while for the shallowest sandy layer, the relation is the opposite—the pore pressure effects are the strongest for the shortest duration waveforms. Those results indicate the importance of factors on the wave propagation other than duration, such as the frequency content of the input or the influence of the pore pressure effects in other layers.

4.4 Effect of the input ground motion

We analyse the impact of the variability of the input ground motion on the resulting non-linear site response. While thick solid and dashed lines (Fig. 9) show the mean and standard deviation over 11 waveforms (Table 4), the thinner lines represent one input each. For effective and total stress analysis, the standard deviation is 31 and 26 per cent, respectively (Table 5), considering the 0.5–20 Hz frequency band. However, when taking into account only the lower frequency band (0.5–5 Hz), the standard deviation for total stress analysis is significantly lower (26 per cent) than for effective stress analysis (39 per cent). It confirms our expectation that the introduction of the pore pressure effects increases the variability of the site response, especially at lower frequencies. We highlight that it is not possible to predict non-linear amplification in 1-D simulations using only one input ground motion. Hence, it is important to use several waveforms with different frequency content, duration, etc. It was shown that 11 waveforms are enough to study linear site response (Perron *et al.* 2022); however, to study the non-linearity and the impact of specific parameters such as intensity or duration, a much broader set of waveforms is needed. Nevertheless, we use the available waveforms (Table 4) to show (Figs D5 and D6) that there is a positive correlation between PGA and duration of the input ground motion and selected output parameters (i.e. PGA at the surface, different non-linearity measures). Such analysis is possible, even though, the waveforms were selected and scaled to fit the elastic response spectrum, but thanks to the implemented search criteria (see Section 3.3), some variability is preserved (Panzera *et al.* 2023a, b, 2024).

4.5 Influence of the dilatancy parameters

As the result of the inversion for dilatancy parameters, we obtain a number of diverse sets of values with different misfits, as shown in Section 4.2. Here, we investigate the sensitivity of the site response due to the variability of the dilatancy parameters. In the previous study (Janusz *et al.* 2022a), the impact of using 30 inverted sets with the lowest misfit was tested for the SLUW site, showing no or a minor influence on the results of wave propagation simulations. We suspect that the best 30 sets are too similar (variability for a single parameter between 0.5 and 5 per cent) to affect the results. We therefore select 30 sets randomly chosen from all inverted sets with the low misfit (e.g. Fig. 7) and test them separately for each sandy layer (Fig. 13, Table 6). Still, the impact on the wave propagation simulations is low, especially for the shallow and deep sandy layers. Even in the case of the middle sandy layer, which shows the highest sensitivity (the mean standard deviation is about 10 per cent); the variability is much below the standard deviation when using different waveforms (Table 5). We also do not observe any major change in the cyclic mobility. We show the variability using only one waveform but we observe similar behaviour for all 11. As the sets derived using the inversion do not allow us to study in detail

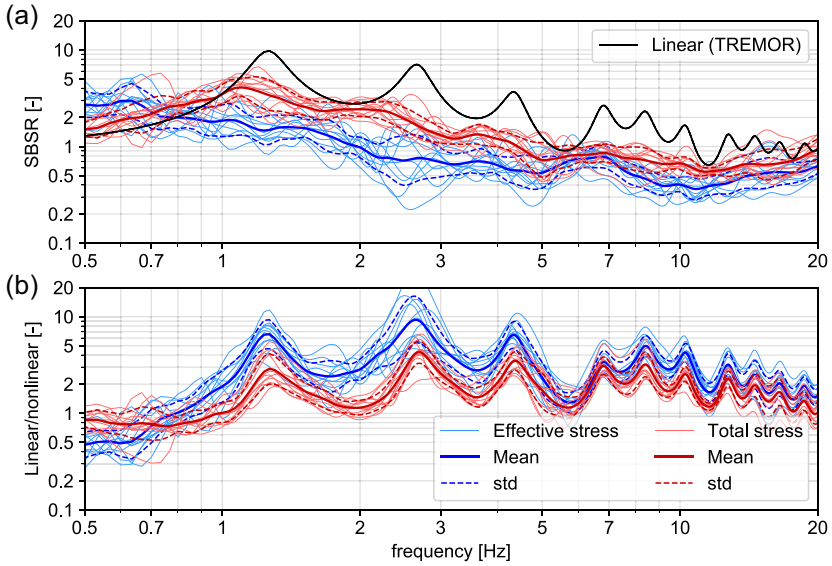

Figure 9. (a) Surface to borehole spectral ratios for linear viscoelastic and non-linear site responses (using respectively effective and total stress analysis) for the SLUW reference model using 11 waveforms (Table 4). Each thin blue and red line corresponds to one waveform. (b) The ratios between linear viscoelastic site response and non-linear site responses.

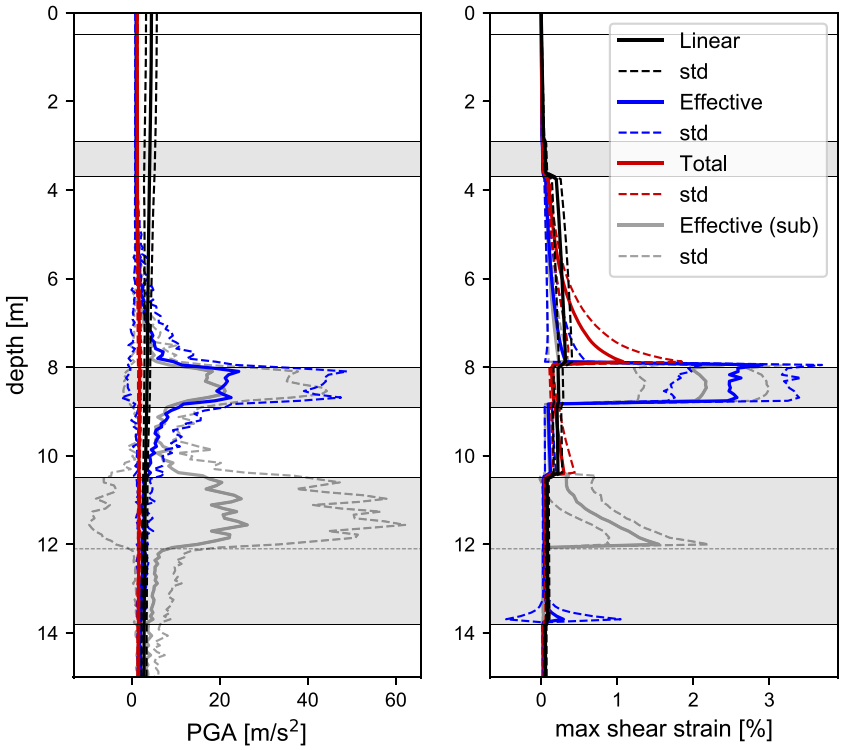

Figure 10. Average and standard deviation for PGA and the maximum shear strain in the first 15 m of the soil model, using 11 waveforms (Table 4). Layering is shown with horizontal lines with sandy layers in grey. The blue and red curves correspond respectively to the effective and total stress analysis for the SLUW reference model. The grey curves are the results when subdividing the deepest sandy layer (dashed horizontal line, explained in Section 5.2).

the influence of the dilatancy parameters on the wave propagation, we create new sets by changing randomly one dilatancy parameter at a time and fixing the rest of the parameters as in Table 2. We draw values within the model search limits (Table 2). Hence, many of these sets are not in the inverted sets for the SLUW site, but such an approach allows us to define the importance of the different dilatancy parameters in the constitutive model.

Using randomized sets of dilatancy parameters as explained above, we have found out that the overall dilatancy w_1 is the most crucial factor. When w_1 reaches high values (>5), it quite effectively reduces the chances for strong pore pressure effects and liquefaction, while low w_1 indicates that these are likely. If w_1 is low, the final phase of the pore pressure excess development is rapid and starts faster. Changing other dilatancy parameters does not affect

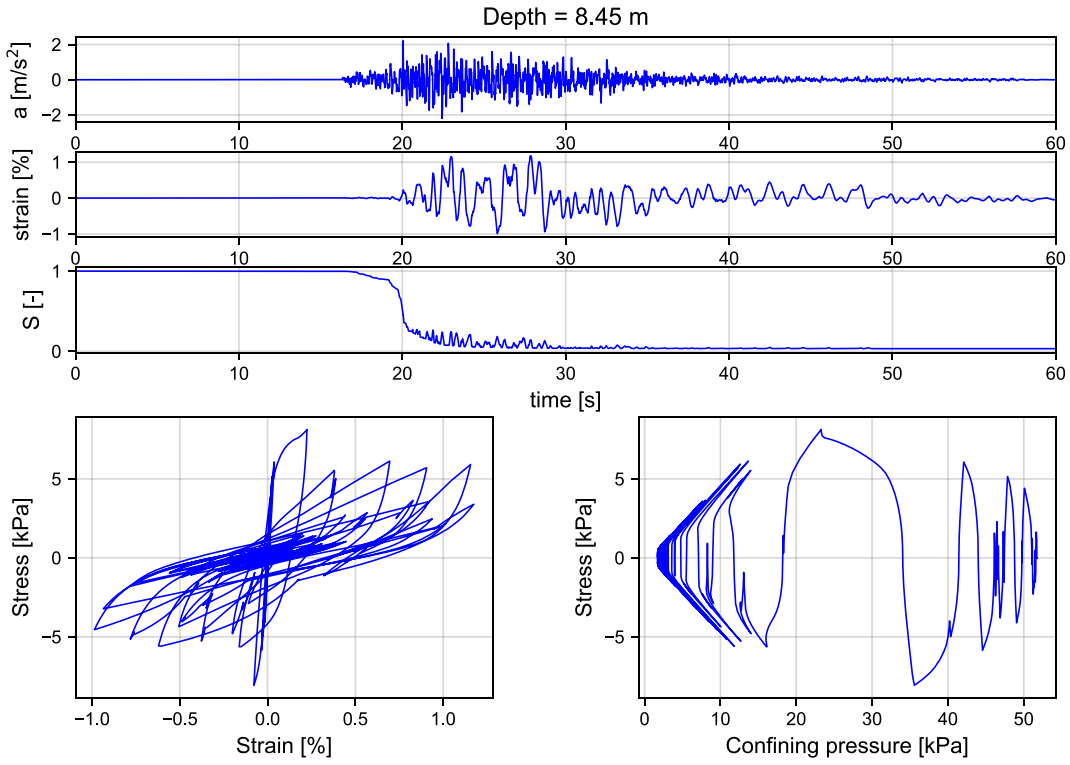

Figure 11. Simulation results at about 8.45 m in the middle sandy layer for waveform no. 6 (Table 4) for the SLUW reference model, where *a* is acceleration and *S* shows the reduction of the initial confining stress.

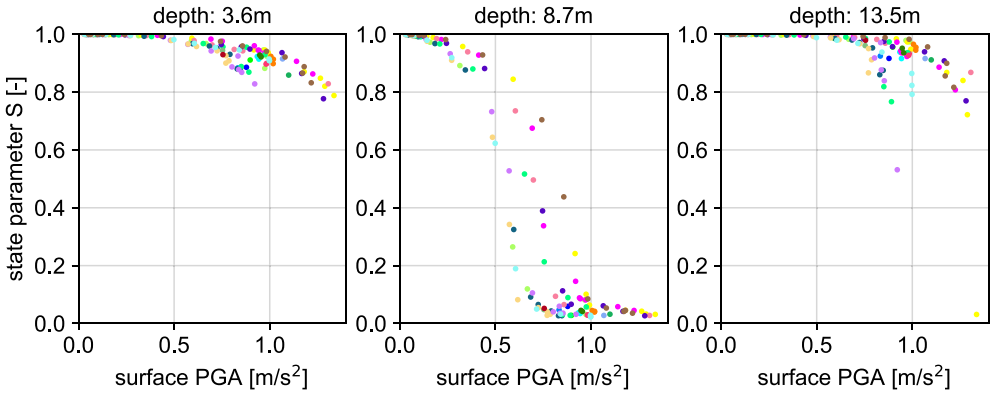

Figure 12. State parameter *S* for each three saturated sandy layers in the SLUW reference soil model compared to the PGA at the surface, using all waveforms from Appendix B. Each dot corresponds to one input ground motion—for the waveforms with the same frequency content but different scaling, they have the same colours.

Table 5. The mean standard deviation for the SBSRs (Fig. 9) for different frequency bands due to the input ground motions (all waveforms from Table 4).

	Mean standard deviation [per cent]	
Frequency [Hz]	0.5–20	0.5–5.0
Effective stress	31	39
Total stress	26	26

the results significantly. Fig. 14 shows the relation between w_1 and state parameter *S* separately for two layers using 11 waveforms from Table 4—in both cases, the only parameter that changes in the whole model is w_1 for a given layer. The relations differ for the deepest and middle sandy layers, with the latter being more susceptible to strong pore pressure effects and liquefaction. The grey rectangles show the w_1 values for the SLUW site derived from the inversion. It explains why the small changes in the dilatancy parameter w_1 do not make a difference. As liquefaction resistance decreases with the number of cycles, the liquefaction should be more likely for a longer duration of shaking. Indeed, we observe to some extent such a relation, at least for the middle sandy layer at 8.45 m depth (Fig. 14, right-hand panel). The lack of correlation for the other layer (Fig. 14, left-hand panel) indicates the importance of other factors; we hypothesise that the frequency content of the input ground motion might play a role here.

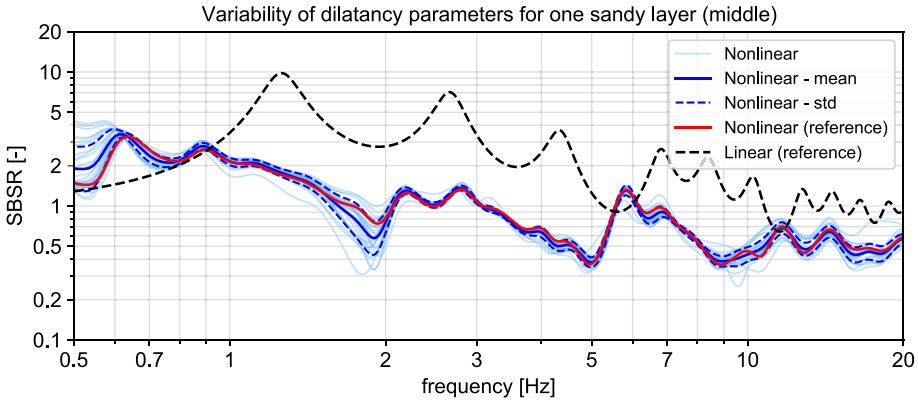

Figure 13. The variability of the results for waveform no. 1 (Table 4) using 30 different sets of dilatancy parameters drawn from the inverted sets for the middle sandy layer. Each thin blue line corresponds to one set of the dilatancy parameters. Red solid and black dashed lines indicate the SLUW reference model.

Table 6. The mean standard deviation for the SBSRs (Fig. 13) for waveform no. 1 (Table 4) due to the 30 different sets of dilatancy parameters.

	Mean standard deviation [per cent]	
Frequency [Hz]	0.5–20	0.5–5.0
Layer 1 (deepest)	2.1	1.3
Layer 2 (middle)	10.6	9.4
Layer 3 (shallowest)	1.1	0.5

Another observation from the analysis using randomized sets of dilatancy parameters is that even if we only change w_1 for one specific layer, we observe a change in the behaviour in the other layers. In some cases, the occurrence of strong pore pressure effects in the deepest layer prevents their development in the layers above, even though w_1 for the latter is low, indicating that the strong pore pressure effects are likely. The energy remains trapped in the layers below. Hence, we cannot consider the layers separately, because the change in the soil behaviour in one layer affects the wave propagation in other layers. Generally, we observe several classes of site response depending on whether the large pore pressure effects are triggered and in which layer—we show an example for one waveform in Fig. 15 and statistics for 11 waveforms (Table 4) in Table 7. We consider here that large pore pressure effects occur if S is less than 0.1. The cases where only the middle sandy layer experiences strong dilatant soil behaviour are dominant (about 70 per cent of the performed tests) and all have a similar shape of SBSR (Fig. 15). The strong soil dilatant behaviour never occurs only when the shortest duration waveform is used as input motion and, as expected, the site response resembles the results of the total stress analysis. If strong pore pressure effects occur only in the deepest sandy layer, more non-linearity is produced than in any other case. We observe it both visually (Fig. 15) and in terms of the amplitude change index (ACI, Table 7). A relatively high ACI is also observed if both the middle and deepest layers are influenced by strong dilatant behaviour. However, the lowest values of ACI are found if only the shallowest layer is affected. Generally, the non-linearity observed at the surface is stronger if the strong pore pressure effects and liquefaction happen in the deeper sections of the soil profile.

4.6 Sensitivity to the soil parameters

We build a soil model mostly from CPT data using empirical relations; however, many such equations exist and we would like to test the influence of the uncertainty of the soil parameters on the overall predicted variability. We create 100 soil models that are constructed by randomly choosing for each model parameter one empirical equation from Table 1, as explained in Section 3.1. We include the uncertainty of V_S, ρ, φ, K_0, Q, cohesion and water table depth. The analysis of the influence of the dilatancy parameters shows that, firstly, the inverted sets are quite consistent (Section 4.2), and secondly, their variability does not affect the results significantly (Section 4.5), especially if w_1 is similar. Hence, we have decided to keep the initial dilatancy parameters (Table 2) for all 100 realisations, because the inversion is a relatively time-consuming and computationally costly process (i.e. for our case study—between 30 and 150 min per run when using cluster and parallel computing).

We plot the results using 100 soil models in Fig. 16 only for one ground motion from Table 4 to focus on the influence of soil parameters. We observe quite a variability of linear viscoelastic soil response with four main types of curves characterized by f_0 at about 1.0, 1.1, 1.2 and 1.3 Hz. The mean f_0 is at about 1.1 Hz, which is slightly different from the reference model (1.2 Hz), which is, however, the most consistent with empirical data for the SLUW site (Fig. 6). Surprisingly, all non-linear SBRS have similar shapes with peaks at the same frequencies, even though the respective linear viscoelastic curves show variability in the resonance frequencies. We suspect that, in our case, the non-linear soil behaviour is strong enough to mask the difference in f_0 visible for linear site response. The variability (Table 8) is higher for effective stress (27 per cent) than for total stress analysis (18 per cent), but lower than the variability due to the different input ground motions (about 30 per cent, Table 5). The reference model for the SLUW site deviates from the mean over 100 realisations, but it is generally within the error bars. The difference could be related to the fact that the reference model is based on V_S from SCPT, while the solely CPT-based velocity models are slightly overrepresented in the selection of the equations (Table 1), used to construct the 100 random models.

We also investigate the effect of changing any individual parameter in the model. We construct, in total, 25 models using the empirical equations from Table 1 (i.e. eight models where V_S profiles vary, three with different φ, etc.). In Appendix E, we show the results for one ground motion from Table 4. We observe that V_S has the most impact on variability (Fig. E1), with some importance of water table depth and K_0 (Figs E2 and E3), while for the rest of the tested parameters (Figs E4–E7), the effect is negligible. It is

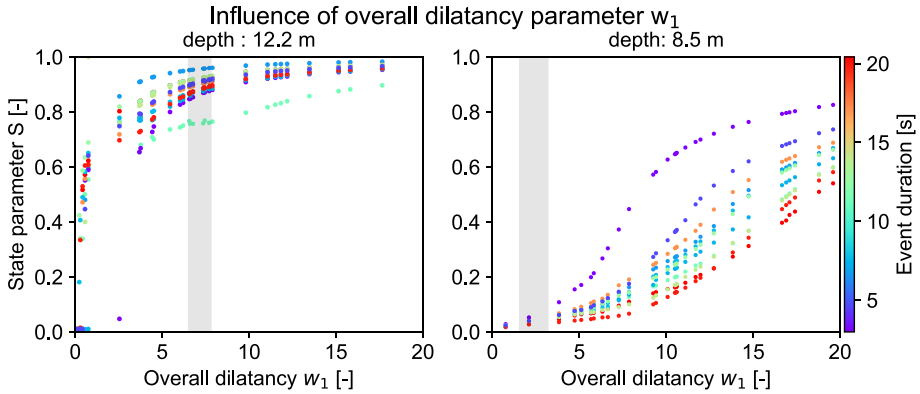

Figure 14. Influence of overall dilatancy parameter w_1 on state parameter S for input ground motions with different durations (Table 4). Each dot corresponds to one simulation using a different value of w_1 and different input ground motion. The grey rectangle shows the range of w_1 from the inversions for the SLUW site at the given depth.

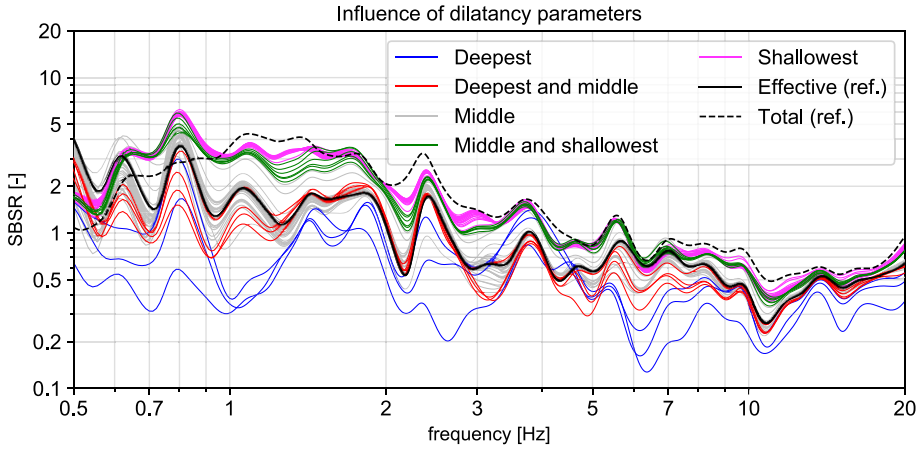

Figure 15. The influence of the dilatancy parameters on SBSRs for waveform no. 3 (Table 4) with the specification by colour, which sandy layers experience strong pore pressure effects defined here as $S < 0.1$. Each colourful line corresponds to one set of dilatancy parameters. Black solid and dashed lines correspond respectively to effective and total stress analysis for the SLUW reference model.

Table 7. Average ACI [per cent] depending on which layers experience strong dilatant soil behaviour ($S < 0.1$) using all waveforms from Table 4. 0 – no strong pore pressure effects, 1 – in the deepest, 2 – in the middle and 3 – in the shallowest sandy layer.

Layer no.	0	1	2	3	1 + 2 + 3	1 + 2	1 + 3	2 + 3
ACI	14.9	34.3	22.5	10.9	22.4	27.6	22.2	13.9

not surprising as the velocity profile is the main input for the wave propagation modelling and the water table depth affects greatly the potential for cyclic mobility. K_0, on the other hand, is decisive in calculating the vertical and horizontal stresses in the soil column, and ultimately the soil strength.

5 DISCUSSION

5.1 Comparison to empirical data

Since no strong motion records are available for the Lucerne area, we cannot directly verify the results, which is a typical problem of assessing non-linear site response in low-to-moderate seismicity areas. Hence, we compare our simulations to empirical data for selected KiK-net sites (Aoi *et al.* 2011, Appendix F), which are to some extent similar to the SLUW site in terms of V_{S30}, f_0, and bedrock condition ($V_{S30} < 350$ m s^{-1}, $f_0 < 2.5$ Hz, bedrock displaying $V_S > 800$ m s^{-1} and at depth < 150 m). Since the SLUW model and selected KiK-net sites are not the same in terms of geological conditions, the following comparison cannot be used as a validation of the procedure. However, it allows assessing if our methodology predicts similar levels of non-linearity and thereby if the results are realistic compared to observations, as we assume that similar sites should not show significantly different non-linear site responses.

We juxtapose simulations for all waveforms from Appendix B with empirical data and compare the relation between PGA recorded at the borehole depth and the surface, and the change in amplitude and shift in frequency in SBSR for frequencies between 0.6 and 20 Hz. The values of the PGA were extracted by taking the geometrical mean of the two horizontal components for each of the considered KiK-net sites. All events recorded between 1997 and 2011 with a minimum magnitude of 2.5 and epicentral distance of less than 200 km were used. Generally, for low to moderate earthquakes, the relation between PGA at the bedrock depth and the surface is linear, while for strong ground motions, it becomes

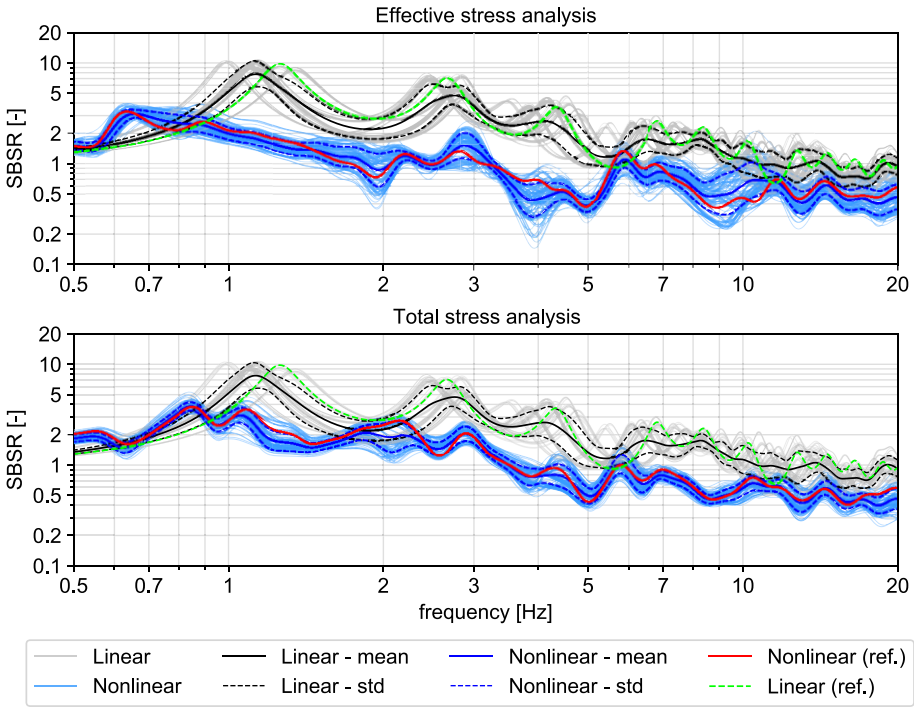

Figure 16. The variability of the results using 100 different soil models for waveform no. 1 (Table 4). Each blue and grey line corresponds to one soil profile. Red and green lines indicate the SLUW reference model.

Table 8. The mean standard deviation for the SBSRs (Fig. 16) for waveform no. 1 (Table 4) due to the 100 different soil models.

	Mean standard deviation [per cent]	
Frequency [Hz]	0.5–20	0.5–5.0
Effective stress	27	22
Total stress	18	19
Linear	27	32

non-linear, that is PGA at the surface is lower than expected from a linear relation. However, the slope of that relation is site-dependent. In order to compare different sites, we need to normalize the PGA at the surface by removing the linear trend. For each KiK-net site and the SLUW site, we fit a line in the linear domain (assumed to be for PGA at the bedrock depth lower than 0.05 m s^{-2}); and then divide all the values by its slope. In that way, for the PGA range where the site response is linear, the PGA values at the surface are aligned around one; while in the non-linear domain, we can compare how much they diverge from the linear trend. Moreover, for each KiK-net site with at least one recording of PGA at the surface higher than 0.01 g, the amplitude change index (ACI) and the frequency shift (S_h) were calculated for all events recorded between 1997 and 2020 with a magnitude above two (Loviknes *et al.* 2022). To describe the relation between ACI and shift in frequency with the recorded PGA at the surface, a hyperbolic tangent function was fitted for each site (Loviknes *et al.* 2022); the coefficients are given in Appendix F.

We plot the PGA at bedrock depth and the surface (Fig. 17), demonstrating that the relation becomes non-linear for high values of PGA at the bedrock depth (>0.1 m s^{-2}) for both empirical and simulated data. They show good consistency in terms of the values and the same deflection point. For higher PGA values (>0.3 m s^{-2}), there are not many recordings for KiK-net sites; however, some points overlap with the simulations (Fig. 17). The S_h (Fig. 18) for KiK-net sites shows a good fit with the simulations for the total

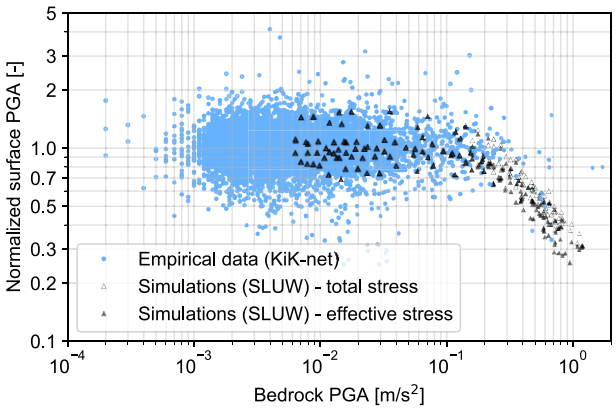

Figure 17. Comparison between PGA recorded at the borehole bottom and the normalized PGA at the surface for several KiK-net sites (blue dots, Appendix F) and simulations for the SLUW reference model (triangles) using all waveforms from Appendix B. Each point corresponds to one input ground motion. The normalization procedure is explained in the text.

stress analysis. In addition, the ACI (Fig. 18) for KiK-net sites and the simulations are within a similar range, even though they display a slightly different trend. However, the ACI is possibly not the optimal tool to compare non-linearity between sites, as it is sensitive to the overall shape and error intervals of the linear site response. For simulations using the effective stress analysis, especially in the case of the occurrence of a strong pore pressure effect and possible liquefaction, the correlation between S_h or ACI and PGA cannot be observed and the values are not comparable to empirical data anymore. There are several possible explanations for that; one is that the modelled soil response may be overestimated or distorted in such cases, inhibiting the comparison to empirical data. However, another reason may be that neither strong dilatant soil behaviour nor liquefaction was triggered for the recorded events at those Kik-net

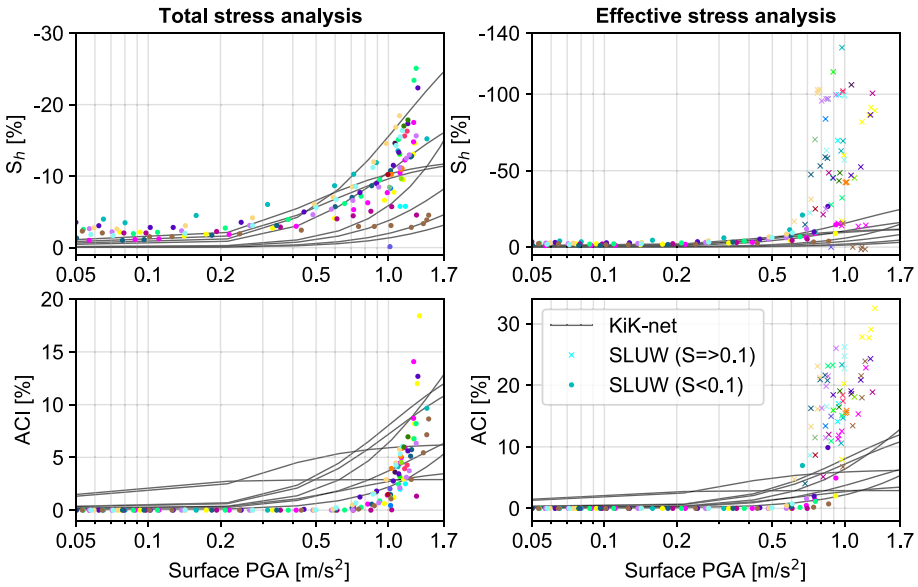

Figure 18. Comparison of the S_h and ACI for several KiK-net sites (grey lines, Appendix F) and simulations for the SLUW reference model (dots and crosses) using all waveforms in Appendix B. Each point corresponds to one input ground motion—for the waveforms with the same frequency content but different scaling, they have the same colours. The crosses represent the cases with the occurrence of the strong pore pressure effects, here defined as the state parameters $S < 0.1$ in at least one layer.

stations. As we have no such information, we would need to make a comparison to the sites with evidence for such soil behaviour. Moreover, the approximated water table depth for the Kik-net sites selected (Appendix F) is generally deeper (a few meters or more) than for the SLUW site (0.5 m), indicating different water pressure conditions, which may also explain the discrepancy observed. Nevertheless, another explanation can be that ACI and S_h may not be a good tool in the case of strong pore pressure effects, as the correlation between PGA and the level of non-linearity disappears. We do not see this difference when comparing PGA at the borehole depth and the surface (Fig. 17), because the effective and total stress analyses do not differ significantly (though, the PGA from effective stress analysis is always slightly smaller); we suspect that PGA is not a good indicator in case of strong pore pressure effects.

5.2 Comparison to classical liquefaction analysis

We have not found a good fit with the empirical data from KiK-net for the simulations with strong pore pressure effects; therefore, we additionally compare the results to a classical method of assessing soil liquefaction resistance using CPT (Youd *et al.* 2001). The constitutive model used in the simulations does not include flow liquefaction, as the state parameter S never reaches zero, meaning that pore pressure excess is never equal to the initial confining pressure; however, it implies the possibility of the liquefaction when S is close to zero. To assess soil liquefaction resistance using the classical method, we first calculate $CRR_{7.5}$ (Robertson & Wride 1998; Robertson 2009b) and compare it to CSR profiles for all 11 waveforms (Table 4), calculated following Youd *et al.* (2001) and using MSF relation from Idriss & Boulanger (2006). The procedure requires defining the magnitude and maximum surface acceleration for each waveform. Although the amplitudes of the 11 waveforms are scaled, we assume that the scaling factors are low enough (they do not exceed 0.5–2) to use the original magnitudes. The PGA at the surface simulated using effective stress analysis is used to estimate the maximum surface acceleration.

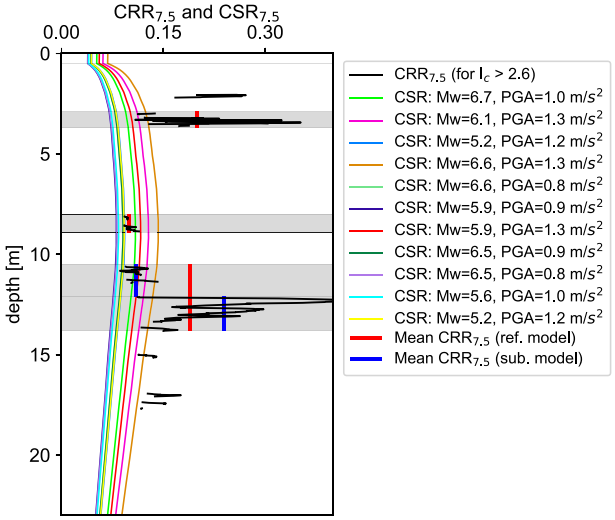

Figure 19. Comparison between $CRR_{7.5}$ and CSR for 11 waveforms (Table 4). The layering is shown with sandy-saturated layers in grey. The vertical lines indicate the mean value of $CRR_{7.5}$ for a given layer for the reference model for the SLUW site (red) and the model with the division of the deepest sandy layer (blue).

Fig. 19 shows a comparison between $CRR_{7.5}$ and CSR for 11 waveforms (Table 4)—if CSR is greater than $CRR_{7.5}$, the applied stress exceeds the soil resistance for liquefaction, and liquefaction can be triggered. According to the performed classical analysis, the middle sandy layer has the potential for liquefaction for several waveforms. In the simulations, this layer experiences strong pore pressure effects and possible liquefaction for all 11 waveforms. The former approach is very simplified; hence, we do not expect the results to be identical. Nevertheless, the comparison shows that our simulation and classical analysis both indicate the possibility of liquefaction in the middle sandy layer. However, the deepest sandy layer does not show strong pore pressure effects in

the simulations, while the classical analysis shows some liquefaction potential. When inverting for dilatancy parameters, we use the mean $CRR_{7.5}$ value for each layer, which, for the deepest sandy layer, overestimates the resistance, especially in the upper part of that layer (Fig. 19). Indeed, if we subdivide the layer and derive separate sets of dilatancy parameters, the upper part of the layer also shows strong deformations (grey line in Fig. 10) due to the dilatant soil behaviour, suggesting the possibility of liquefaction. However, the effect of an additional layer with strong pore pressure effects is not visible at the surface; SBSRs and PGA are almost the same (about 1.1 m s^{-2}, Fig. 10). Nevertheless, although the effect on the surface is negligible, the damage to underground infrastructure will be significantly different in both considered examples. Hence, it is important not to merge the liquefaction-prone layers characterized by different $CRR_{7.5}$.

5.3 On the uncertainty and usability of the method

All steps of the presented procedure involve significant uncertainties. We have focused on analysing the impact of the variability of the input ground motion and the uncertainty of the soil parameters, including the dilatancy parameters because we have suspected that they are the most influential. We observe a significant spread when investigating the impact of the soil parameters and input ground motion separately (Fig. 9, Fig. 16); nevertheless, the site response functions are consistent with each other with only a few outliers. However, if we consider all the uncertainties together, the total error bars can be substantial. Still, in our opinion, the uncertainties are acceptable and manageable—we can assess the extent of the resulting variability and quantify it by including a large number of input ground motions and soil models, and derive the statistical value of the site-specific non-linear response that can be then used to refine the seismic hazard and risk assessment at a local scale. The subsequent error bars should be also considered. The method proposed establishes a useful tool to estimate the non-linear soil response in the areas with limited data. However, the logical next step should include the verification using strong motion and laboratory data. The cost of drilling and collecting soil samples and repeating the procedure in the area with observations of the non-linearity from earthquake data might be justified, as we show that the results are realistic (Sections 5.1 and 5.2) and the uncertainties are acceptable (Sections 4.4–4.6). However, only the comparison with the earthquake data can provide the most definite validation of the method, while laboratory data is also an estimation. Another reason to pursue the procedure is that the potential non-linear effects are difficult to approximate using other conventional approaches in areas similar to Lucerne, especially because the effective stress analysis has to be applied due to the geological conditions. In addition, the importance of considering the pore pressure effects that have been observed (Section 4.3). The other techniques require more parameters than the constitutive model used, including, for example, laboratory-derived parameters that are not always available. Another solution that is commonly applied in such cases is to assume the parameters based on proxies or literature values; however, the uncertainty will be even higher. Using CPT fills the gap between those two approaches, providing a relatively low-cost and fast tool, as the datasets of CPT measurements exist in many areas (e.g. New Zealand Geotechnical Database, NZGD 2023). Moreover, it provides *in situ* information about the soil parameters, allowing for site-specific estimation of site response. Alternatively, we can apply the classical analysis of the liquefaction resistance as in Section 5.2 but the advantage of the multi-step procedure presented is that it provides full-time histories of acceleration, strain, and pore pressure instead of a simple estimation of the liquefaction potential. One of the limitations of the approach presented is that the constitutive model does not consider flow liquefaction; however, different models, also with different rheology, can be incorporated.

We cannot directly compare the influence from input ground motion and soil model parameters, as we have not performed the full sensitivity analysis; however, we show a sufficient overview of the variability. We highlight that the variability of the input ground motion plays a major role. Therefore, even with the most realistic and complete soil model, the variability of the resulting site response cannot be reduced significantly, since it depends strongly on the input waveforms, it is part of the aleatoric component of the uncertainty. We recommend using many different waveforms in the analysis—probably 11 are not enough to fully capture the variability. The impact of the uncertainty of the soil parameters is significant but within a reasonable range, especially the influence of the dilatancy parameters variability, derived from inversion, which is of minor importance. Therefore, only some distinctive feasible combinations need to be tested to account for that uncertainty. In addition, as we earlier demonstrated (Section 4.5), it is mostly the overall dilatancy w_1 in the constitutive model that controls the potential for strong pore pressure effects and liquefaction. It reduces the number of unknowns to some extent, especially since w_1 is often well-constrained in the inversion. Nevertheless, the inversion procedure for deriving the dilatancy parameters from CPT remains another source of uncertainty in the workflow, as we do not have empirical data (geotechnical laboratory tests or strong motion data) to test our results. However, the comparison to laboratory-derived parameters would not be ultimately decisive in confirming or denying the applicability of the method because the soil samples may not reflect *in situ* conditions or be representative of the entire soil profile. We propose to use CPT data, as it is an *in situ* test able to investigate continuously the surficial soil in a significant depth range and it constitutes a good approximation for the dilatancy parameters. The inversion procedure was initially created as an alternative to the trial-and-error method to derive the dilatancy parameters from laboratory data (Roten *et al.* 2011)—here CPT data is used instead and was also tested using synthetic examples (Janusz *et al.* 2022a, b). In addition, the procedure was used to invert the dilatancy parameters from strong motion data in Japan (Roten *et al.* 2014), the simulations using the minimum misfit solution from the inversion show good agreement with the observed accelerograms. The LRC curve based on the dilatancy parameters inverted from earthquake data was also compared to the LRC derived from CPT for one site in Japan (Roten *et al.* 2014), demonstrating that they are somehow similar. In addition, we performed some indirect comparison—the classical analysis of the liquefaction resistance (Section 5.2) predicts the liquefaction for the same layers.

Although we perform quite an extensive analysis of the influence of different realisations of the soil model on the results, we do not fully capture the epistemic uncertainty because—due to time and computational constraints—we investigate a limited number of parameter combinations rather than building a whole logic tree. Furthermore, we test only one soil constitutive model. Thus, the epistemic uncertainty may increase when using other models with other parameters that are related to them. Indeed, we do not include all possible empirical approximations that can be derived from CPT or seismic data, just some subjectively selected ones, which is another source of uncertainty. In that way, we may also have

overrepresented some types of relations. In addition, those empirical equations alone involve substantial uncertainties (Robertson & Wride 1998; Robertson 2009a). They are typically based on the correlations for the datasets for specific areas and materials. Here, we try to select the relations derived from large compilations of samples and appropriate for a wide range of sediments to decrease subjectivity; in addition, we computed the average over different realisations. We also test only one version of MSF while several are available in the literature (e.g. Youd *et al.* 2001; Idriss & Boulanger 2006; Boulanger & Idriss 2015) and their effect on the inversion of the dilatancy parameters should be considered. We have also made some oversimplifications by assuming that dilatancy parameters do not change for various soil models. In addition, we investigate the influence of only selected aspects; we mostly neglect the effect of the deep part of the profile (>30 m) or the influence of dividing the soil model into different numbers of layers. Moreover, we do not consider the spatial variability of the soil response in the area, which can be substantial due to local heterogeneities; however, such analysis will be performed in the future. We perform a 1-D study, even though; 2-D/3-D site effects may affect the area. However, first, the 1-D approximation can already explain the empirical site response in the linear domain to some extent, as shown in Fig. 6. In addition, comparison to Kik-net data shows that our methodology allows predicting similar levels of non-linearity, at least for cases without the occurrence of large pore pressure effects, even though it is only a 1-D approximation. Secondly, the main aim of this study is to assess the usability and sensitivity of the method. Hence, we have decided that 1-D approximation is sufficient for that purpose, especially because building a detailed 2-D model is a demanding task, requiring site characterization measurements and drilling, while applying a too simplistic 2-D model based mostly on assumption would introduce larger uncertainties. However, 1-D simulations may be not enough in some areas with strong 2-D/3-D effects. We could not investigate all feasible features and impacts and some could be underestimated or difficult to assess. Still, our sensitivity analysis provides a good overview of the variability. Moreover, based on the analysis performed, we suspect that including more variables and combinations that are realistic would not change the results significantly, especially in terms of mean or median value; however, it would increase the final variability and error bands.

6 CONCLUSIONS

We presented a multi-step procedure that allows estimating soil non-linearity in the absence of strong-motion recordings and laboratory data, which is especially suitable in areas with low-to-moderate seismic hazard. It relies on data from CPT surveys and allows approximating the level of strain, assessing the pore pressure effects, and providing acceleration time histories. The workflow proposed draws on three main pre-existing tools: (a) derivation of the soil parameters from CPT data, (b) inversion for the dilatancy parameters using CPT and (c) non-linear wave propagators. The method potentially bridges the gap between, on one side, a detailed but cost- and time-consuming assessment of soil non-linearity with laboratory tests, and, on the other side, the adoption of shear modulus decay and damping curves from literature, when geotechnical data are not available. The workflow provides an alternative to established methods in areas similar to Lucerne where limited data is available. First, the constitutive model requires a relatively small number of input parameters. Secondly, the method is relatively cheap and fast as soil samples are not necessary, and CPT data is becoming more and more available in urban areas. It allows estimating the soil parameters *in situ* and avoiding sampling problems typical for laboratory measurements. In addition, the inversion for the dilatancy parameters is less time-consuming than the commonly used trial-and-error approach.

However, due to a lack of laboratory and strong motion data, the results are not directly verified and provide only a first-order approximation of non-linearity. Full validation is necessary, especially using the observation of the non-linear soil behaviour from earthquake data. However, a comparison of the results to the strong motion data from KiK-net shows that the methodology predicts similar levels of non-linearity and hence provides a realistic estimate of the non-linear site response, at least for cases without the occurrence of the large pore pressure effects. Nevertheless, the simulations that consider pore pressure effects show the liquefaction potential similar to the classical method for liquefaction resistance evaluation and the liquefaction PGA threshold reported in the literature.

We analysed the impact of the input ground motion and the uncertainty of soil model parameters, including the dilatancy parameters, indicating that the resulting variability is significant but acceptable, allowing estimating the soil response with reasonable error bars. In particular, the input ground motions are an important source of the variability, pointing out a need to run simulations using many different waveforms. We observed the correlation between the intensity and duration of the ground motion and the degree of non-linearity. The partial sensitivity analysis of soil parameters shows their significant influence on the simulated non-linear site response but the results using different soil models are consistent with each other. The results are more sensitive to some parameters such as V_S or water table depth, while the influence of, for example, the dilatancy parameters inverted from CPT is less significant. However, the inversion procedure is non-linear and non-unique, giving often more than one solution with an associated large uncertainty in some cases.

The simulated soil response is strongly dependent and controlled by the occurrence of the strong pore pressure effects and possible liquefaction. For some combinations of the soil parameters, it becomes inevitable above some PGA threshold (1.0 $\mathrm{m\,s^{-2}}$ at the surface in our case study). We found that it is the overall dilatancy parameter w_1 that mostly controls the possibility of the strong dilatant soil behaviour in the constitutive model, where low values (<5) make the large pore pressure effects and liquefaction very likely. The low value of w_1 in the model means that the development of the pore pressure excess is relatively rapid and the build-up starts early; hence, w_1 can be equated to similar parameters in other constitutive models that are responsible for such behaviour.

The method can be applied in a variety of areas; here, we perform analysis for Lucerne, providing an estimation of the non-linearity impact. We imply a high probability of strong non-linearity with extensive damping of the ground motion and shift of the predominant frequency (1.2 Hz) towards lower frequencies for the tested site. The threshold found for non-linearity is about 0.1 $\mathrm{m\,s^{-2}}$ for input PGA at bedrock depth. Our results suggest a high probability of the strong pore pressure effects and liquefaction for at least one sandy-saturated layer for the waveforms that correspond to the seismic hazard with a return period of about 975 yr. Those findings should be used to refine the local seismic hazard and risk assessment in Lucerne and Switzerland, as for now; the non-linear soil behaviour analysis is not commonly included. However, this study aimed to test the procedure and its sensitivity; hence, the results can be treated only as a preliminary estimation for one specific site and

the particular set of the input motions (i.e. for a return period of 975 yr). We do not capture the spatial variability of soil response; in addition, it is a 1-D approximation. In the future, the application at the local scale (Lucerne, Visp) is planned to estimate the impact of the non-linearity on the local seismic hazard and risk assessment, using many sites and more input motions, also for different hazard levels. We would also include 2-D and 3-D soil models.

ACKNOWLEDGMENTS

This study is part of the PhD project of Paulina Janusz that was funded by the European Union's Horizon 2020 ITN program in the framework of the URBASIS-EU project (grant agreement no 813137). The input ground motions were obtained as part of the project 'Database for design-compatible waveforms' funded by the Swiss Federal Office for the Environment (FOEN). The inversion and the numerical simulations were performed on the Euler cluster operated by the High-Performance Computing group at ETH Zürich. The authors would like to thank Miroslav Hallo and Vincent Perron for their comments and advice, as well as the editors and reviewers for their help in improving this paper.

AUTHOR CONTRIBUTIONS

Paulina Janusz (Conceptualization, Methodology, Software, Writing, Visualization, Formal Analysis); Paolo Bergamo (Supervision, Methodology, Formal Analysis); Luis Fabian Bonilla (Supervision, Software, Methodology); Francesco Panzera (Formal Analysis); Daniel Roten (Software, Methodology); Karina Loviknes (Formal analysis) and Donat Fäh (Supervision, Funding acquisition, Project administration, Conceptualization)

SUPPORTING INFORMATION

Supplementary data are available at *GJIRAS* online.

Table A1. Input soil model for the SLUW site (reference model).
Table A2. Input parameters for NOAH.
Figure A1. CPT data and interpretation for the SLUW site (reference model).
Table B1. Metadata of all input ground motions used in the study.
Figure B1–B4. Spectral acceleration of the scaled waveforms from Table B1.
Figure C1. Misfit of the inverted sets of dilatancy parameters for the deepest sandy layer.
Figure C2. Misfit of the inverted sets of dilatancy parameters for the shallowest sandy layer.
Figure D1. State parameter S for each of the three saturated sandy layers compared to the PGA in the layer.
Figure D2. State parameter S for each of the three saturated sandy layers site compared to the strain in the layer.
Figure D3. State parameter S for each of the three saturated sandy layers compared to the PGA of input ground motion.
Figure D4. State parameter S for each of the three saturated sandy layers compared to the duration of the input ground motion.
Figure D5. PGA and duration of the input ground motion compared to selected results of the simulation (i.e. PGA at the surface, ACI, *Sh*) for effective stress analysis.
Figure D6. PGA and duration of the input ground motion compared to selected results of the simulation (i.e. PGA at the surface, ACI, *Sh*) for total stress analysis.
Figure E1. The variability of the results due to the different empirical relations to derive V_S (Table 1) for waveform no. 1 (Table 4).
Figure E2. The variability of the results due to the different water table depths (Table 1) for waveform no. 1 (Table 4).
Figure E3. The variability of the results due to the different empirical relations to derive K_0 (Table 1) for waveform no. 1 (Table 4).
Figure E4. The variability of the results due to the different empirical relations to derive density (Table 1) for waveform no. 1 (Table 4).
Figure E5. The variability of the results due to the different empirical relations to derive Q (Table 1) for waveform no. 1 (Table 4).
Figure E6. The variability of the results due to the different empirical relations to derive friction angle (Table 1) for waveform no. 1 (Table 4).
Figure E7. The variability of the results due to the different empirical relations to derive cohesion (Table 1) for waveform no. 1 (Table 4).
Table F1. Selected KiK-net sites used in the study to compare the results to the relation between PGA recorded at the borehole and PGA recorded at the surface.
Table F2. Selected KiK-net sites used in the study to compare the results of the change in amplitude (ACI) and shift in frequency (Sh) in SBSR ratios.

Please note: Oxford University Press are not responsible for the content or functionality of any supporting materials supplied by the authors. Any queries (other than missing material) should be directed to the corresponding author for the article.

DATA AVAILABILITY

Earthquake waveforms for the SSMNet station SLUW are available from the Swiss Strong Motion Portal (SSMP, strongmotionportal.seismo.ethz.ch; doi. org/10.12686/sed/networks/ch) maintained by Swiss Seismological Service (SED) at ETH. The instructions on how to access the data can be found at seismo.ethz.ch/en/research-and-teaching/products-software/waveform-data. Earthquake data for the KiK-net sites are available from the National Research Institute for Earth Science and Disaster Prevention (kyoshin.bosai.go.jp). Site characterization data for the SLUW site are drawn from the Site Characterization Database for Seismic Stations in Switzerland created by SED (stations.seismo.ethz.ch, doi.org/10.12686/sed-stationcharacterizationdb). Dataset of selected design-compatible waveforms for microzonation studies used for simulations are available (doi:10.3929/ethz-b-000633618). The topographic and geological maps are reproduced with the permission of the Federal Office of Topography Swisstopo (JA100120) and can be found at map.geo.admin.ch. The hydrological maps are available from the Geoportal of Kanton Luzern (map.geo.lu.ch/gewaesser/grundwasser). The figures and maps were created using the Matplolib python library (matplotlib.org) and QGIS (qgis.org).

REFERENCES

Ancheta, T. *et al.*, 2014. NGA-West2 database, *Earthq. Spectra,* **30,** 989–1005.
Aoi, S., Kunugi, T., Nakamura, H. & Fujiwara, H., 2011. Deployment of new strong motion seismographs of K-NETK-NETand KiK-net, in *Earthquake*

Data in Engineering Seismology: Predictive Models, Data Management and Networks Geotechnical, Geological, and Earthquake Engineering, Vol., **14,** pp. 167–186, eds Akkar, S., Gülkan, P. & Eck, T. van, Springer Netherlands. doi:10.1007/978-94-007-0152-6_12.

Arias, A., 1970. A measure of earthquake intensity, in *Seismic Design for Nuclear Power Plants,* pp. 438–483, ed. Hansen, Robert J., MIT Press.

Baker, J.W. & Lee, C., 2018. An improved algorithm for selecting ground motions to match a conditional spectrum, *J. Earthq. Eng.,* **22,** 708–723.

Bard, P.-Y. & Bouchon, M., 1985. The two-dimensional resonance of sediment-filled valleys, *Bull. seism. Soc. Am.,* **75,** 519–541.

Bardet, J.P., 1986. Bounding surface plasticity model for sands, *J. Eng. Mech.,* **112,** 1198–1217.

Beresnev, I.A. & Wen, K.-L., 1996. Non-linear soil response—a reality?, *Bull. seism. Soc. Am.,* **86,** 1964–1978.

Bergamo, P., Panzera, F., Danciu, L. & Fäh, D., 2021. Basis for the determination of waveforms for the sites of dams in Switzerland—subproject 1: disaggregation of seismic hazard for return periods of 1000, 5000, 10000 years—disaggregation dataset, Swiss Seismological Service (SED), ETH Zurich. doi:10.3929/ethz-b-000521974

Bergamo, P., Panzera, F., Danciu, L. & Fäh, D., 2022. Database for design-compatible waveforms. Deliverable: disaggregation of the seismic hazard at return periods of 475 and 975 years, Swiss Seismological Service (SED), ETH Zurich. doi:10.3929/ethz-b-000579210

Bonilla, L.F., 2001. *NOAH: User's Manual, Institute for Crustal Studies,* University of California, Santa Barbara, USA, Institut de Radioprotection et de Surete Nucleaire, France.

Bonilla, L.F., Archuleta, R. & Lavallée, D., 2005. Hysteretic and dilatant behavior of cohesionless soils and their effects on non-linear site response: field data observations and modeling, *Bull. seism. Soc. Am.,* **95,** 2373–2395.

Bonilla, L.F., Guéguen, P. & Ben-Zion, Y., 2019. Monitoring coseismic temporal changes of shallow material during strong ground motion with interferometry and autocorrelation, *Bull. seism. Soc. Am.,* **109,** 187–198.

Boulanger, R.W. & Idriss, I.M., 2015. Magnitude scaling factors in liquefaction triggering procedures, *Soil Dyn. Earthq. Eng.,* **79,** 296–303.

Boulanger, R.W. & Ziotopoulou, K., 2015. PM4Sand (Version 3): a sand plasticity model for earthquake engineering applications (Report No. UCD/CGM-15/01), Center for Geotechnical Modeling, Department of Civil and Environmental Engineering, University of California, Davis, CA.

Brocher, T., 2007. Key elements of regional seismic velocity models for long period ground motion simulation, *J. Seismol.,* **12,** 217–221.

Bundesamt für Statistik., 2023. Ständige Wohnbevölkerung nach staatsangehörigkeitskategorie, Geschlecht und Gemeinde, Provisorische Jahresergebnisse, 2022–2022. Retrieved 15 June 2023, from https://www.bfs.admin.ch/asset/de/24325503

Cauzzi, C. & Clinton, J., 2013. A high- and low-noise model for high-quality strong-motion accelerometer stations, *Earthq. Spectra,* **29,** 85–102.

Chandra, J., Guéguen, P. & Bonilla, L.F., 2016. PGA-PGV/Vs considered as a stress–strain proxy for predicting non-linear soil response, *Soil Dyn. Earthq. Eng.,* **85,** 146–160.

Chandra, J., Guéguen, P., Steidl, J.H. & Bonilla, L.F., 2015. In situ assessment of the G–γ curve for characterizing the non-linear response of soil: application to the Garner Valley Downhole array and the Wildlife Liquefaction Array, *Bull. seism. Soc. Am.,* **105,** 993–1010.

Dafalias, Y. & Manzari, M., 2004. Simple plasticity sand model accounting for fabric change effects, *J. Eng. Mech.-ASCE,* **130,** 622–634.

Day, S.M., 1998. Efficient simulation of constant Q using coarse-grained memory variables, *Bull. seism. Soc. Am.,* **88,** 1051–1062.

Diehl, T. *et al.*, 2014. Earthquakes in Switzerland and surrounding regions during 2013, *Swiss J. Geosci.,* **107,** 359–375.

Edwards, B., Michel, C., Poggi, V. & Fäh, D., 2013. Determination of site amplification from regional seismicity: application to the Swiss national seismic networks, *Seismol. Res. Lett.,* **84,** 611–621.

Elgamal, A., Yang, Z. & Parra, E., 2002. Computational modeling of cyclic mobility and post-liquefaction site response, *Soil Dyn. Earthq. Eng.,* **22,** 259–271.

Eurocode 8., 2023. Design of structures for earthquake resistance, general rules, seismic actions and rules for buildings, European Standard (Draft FprEN 1998-1-1:2024), European Committee for Standardization (CEN).

Fäh, D. *et al.*, 2011. ECOS-09 Earthquake Catalogue of Switzerland release 2011 (Report No. SED/ECOS/R/001/20110417), Swiss Seismological Service (SED), ETH Zurich. Retrieved from http://ecos09.seismo.ethz.ch.

Field, E.H. *et al.*, 1998. Non-linear site response: where we're at (A report from a SCEC/PEER seminar and workshop), *Seismol. Res. Lett.,* **69,** 230–234.

Geoportal, Kanton Luzern., 2023. Grundwasser. Retrieved July 7, 2023, from https://map.geo.lu.ch/gewaesser/grundwasser.

Gisler, M., Fäh, D. & Kästli, P., 2004. Historical seismicity in Central Switzerland, *Eclogae Geol. Helv.,* **97,** 221–236.

Guéguen, P., Bonilla, L.F. & Douglas, J., 2018. Comparison of soil non-linearity (In Situ Stress–Strain Relation and G/Gmax Reduction) observed in strong-motion databases and modeled in ground-motion prediction equations, *Bull. seism. Soc. Am.,* **109,** 178–186.

Hegazy, Y.A. & Mayne, P., 1995. Statistical correlations between Vs and CPT data for different soil types, *Cone Penetration Testing (CPT'95),* **2,** 173–178.

Hegazy, Y.A. & Mayne, P., 2006. A global statistical correlation between shear wave velocity and cone penetration data, in *Presented at the GeoShanghai International Conference 2006,* pp. 243–248, Geotechnical Special Publication.

Héloïse, C., Bard, P.-Y. & Rodriguez-Marek, A., 2012. Site effect assessment using KiK-net data: part 1. A simple correction procedure for surface/downhole spectral ratios, *Bull. Earthq. Eng.,* **10,** 421–448.

Hobiger, M. *et al.*, 2021. Site characterization of Swiss strong-motion stations: the benefit of advanced processing algorithms, *Bull. seism. Soc. Am.,* **111,** 1713–1739.

Iai, S., Matsunaga, Y. & Kameoka, T., 1990. Parameter identification for a cyclic mobility model, Report of the Port and Harbour Research Institute, Vol. **29,** No. 4, pp. 57–83.

Idriss, I.M. & Boulanger, R.W., 2006. Semi-empirical procedures for evaluating liquefaction potential during earthquakes, *Soil Dyn. Earthq. Eng.,* **26,** 115–130.

Ishihara, K. & Towhata, I., 1982. Dynamic response analysis of level ground based on the effective stress method, in *Soil Mechanics—Transient and Cyclic Loads,* pp. 133–172, eds Pande, G.N. & Zienkiewicz, O.C., Wiley.

Janusz, P., Bonilla, L.F. & Fäh, D., 2022a. URBASIS Deliverable: a case study on non-linear soil response in urban areas (URBASIS deliverable, Work Package: WP3 No. D3.2), Swiss Seismological Service (SED), ETH Zurich. doi:10.3929/ethz-b-000575536

Janusz, P., Bonilla, L.F., Perron, V. & Fäh, D., 2022b. Calibration of soil dilatancy parameters using CPT data—the case of Lucerne in central Switzerland, in *Proceedings of the 3rd European Conference on Earthquake Engineering and Seismology –3ECEES,* pp. 4747–4756, Editura Conspress.

Janusz, P., Perron, V., Knellwolf, C. & Fäh, D., 2022c. Combining earthquake ground motion and ambient vibration recordings to evaluate a local high-resolution amplification model—insight from the Lucerne area, Switzerland, *Front. Earth Sci.,* **10**

Keller & Lorenz, A.G., 2010. *Baugrund-Hinweiskarte,* Blatt 1150 Luzern, Erläuterungen (Bericht No. 6 4199), Luzern.

Kjartansson, E., 1979. Constant Q-wave propagation and attenuation, *J. geophys. Res.,* **84,** 4737–4748.

Konno, K. & Ohmachi, T., 1998. Ground-motion characteristics estimated from spectral ratio between horizontal and vertical components of microtremor, *Bull. seism. Soc. Am.,* **88,** 228–241.

Kramer, S.L., 1996. Geotechnical earthquake engineering, in *Prentice-Hall International Series in Civil Engineering and Engineering Mechanics,* 1st edn, ed. Hall, W. J., Pearson.

Kremer, K., Gassner-Stamm, G., Grolimund, R., Wirth, S.B., Strasser, M. & Fäh, D., 2020. A database of potential paleoseismic evidence in Switzerland, *J. Seismol.,* **24**(2), 247–262.

Kulhawy, F.H. & Mayne, P., 1990. Manual on Estimating Soil Properties for Foundation Design sign (EPRI EL-6800 Project 1493-6 No. Final Report), Cornell University.

Lade, P.V., 2005. Overview of constitutive models for soils, in *ASCE Geotechnical Special Publications No. 128, Soil Constitutive Models: Evaluation, Selection, and Calibration,* pp. 1–34, eds Yamamuro, Jerry A. & Kaliakin, Victor N., GeoFrontiers, American Society of Civil Engineers.

Liao, T., Mayne, P., Tuttle, M., Schweig, E. & Van Arsdale, B.R., 2002. CPT site characterization for seismic hazards in the New Madrid seismic zone, *Soil Dyn. Earthq. Eng.,* **22,** 943–950.

Loviknes, K., Bergamo, P., Fäh, D. & Cotton, F., 2022. Systematic assessment of non-linear soil behaviour at KiK-net sites (Japan) and correlation with geotechnical and geological indicators, in *3rd European Conference on Earthquake Engineering and Seismology –3ECEES,* pp. 4807–4814, Editura Conspress.

Luzi, L. *et al.*, 2016. The engineering strong-motion database: a platform to access Pan-European accelerometric data, *Seismol. Res. Lett.,* **87,** 987–997.

Masing, G., 1926. Eigenspannungen und verfestigung beim messing, in *Proceedings of the 2nd International Congress of Applied Mechanics,* Zurich, pp. 332–335.

Mayne, P. & Kulhawy, F.H., 1983. K-OCR relationships in soil, *Int. J. Rock Mech. Min. Sci. Geomech. Abstr.,* **20**. 851–869.

Mayne, P., 2014. Interpretation of geotechnical parameters from seismic piezocone tests, in *Proceedings of the 3rd International Symposium on Cone Penetration Testing (CPT14),* Las Vegas, Nevada, 12–14 May 2014, pp. 47–73.

Mayoraz, J., Lacave, C. & Duvernay, B., 2016. Erdbeben: karten der Baugrundklassen, Erstellung und Verwendung. Umwelt-Wissen Nr. 1603: 48 S, Bern: Bundesamt für Umwelt BAFU. Retrieved from www.bafu.admin.ch/uw-1603-d.

Mesri, G. & Abdel-Ghaffar, M.E.M., 1993. Cohesion intercept in effective stress-stability analysis, *J. Geotech. Eng.,* **119,** 1229–1249.

Michel, C., Edwards, B., Poggi, V., Burjánek, J., Roten, D., Cauzzi, C. & Fäh, D., 2014. Assessment of site effects in alpine regions through systematic site characterization of seismic stations, *Bull. seism. Soc. Am.,* **104,** 2809–2826.

Nagashima, F. & Kawase, H., 2021. The relationship between vs, vp, density and depth based on PS-logging data at K-NET and KiK-net sites, *Geophys. J. Int.,* **225,** 1467–1491.

NCHRP., 2007. *Cone Penetrating Testing, A Synthesis of Highway Practice*. National Cooperative Highway Research Program, Transportation Research Board of the National Academies. doi:10.17226/23143.

NZGD., 2023. The New Zealand Geotechnical Database, Retrieved from https://www.nzgd.org.nz.

Olsen, K.B., 2000. Site amplification in the Los Angeles Basin from three-dimensional modeling of ground motion, *Bull. seism. Soc. Am.,* **90,** S77–S94.

Onyelowe, K.C., Ebid, A.M., Ramani Sujatha, E., Fazel-Mojtahedi, F., Golaghaei-Darzi, A., Kontoni, D.-P.N. & Nooralddin-Othman, N., 2023. Extensive overview of soil constitutive relations and applications for geotechnical engineering problems, *Heliyon,* **9,** e14465, doi:10.1016/j.heliyon.2023.e14465.

Panzera, F., Bergamo, P. & Fäh, D., 2023a. Database for design-compatible waveforms (Report), Swiss Seismological Service (SED), ETH Zurich. doi:10.3929/ethz-b-000633297.

Panzera, F., Bergamo, P. & Fäh, D., 2023b. Dataset of selected design-compatible waveforms for microzonation studies, Swiss Seismological Service (SED), ETH Zurich. doi:10.3929/ethz-b-000633618.

Panzera, F., Bergamo, P., Danciu, L. & Fäh, D., 2024. Investigating worldwide strong motion databases to derive a collection of free-field records to select design-compatible waveforms for Switzerland, *Bull. Earthq. Eng.,* **22,** 4843–4872.

Papadopoulos, A.N. *et al.*, 2023. The Earthquake Risk Model of Switzerland ERM-CH23. Natural Hazards and Earth System Sciences (NHESS) [accepted]. EGUsphere [preprint]. doi:10.5194/egusphere-2023-1504.

Perron, V., Bergamo, P. & Fäh, D., 2022. Evaluating the minimum number of earthquakes in empirical site response assessment: input for new requirements for microzonation in the Swiss building codes, *Front. Earth Sci.,* **10,** doi:10.3389/feart.2022.917855.

Poggi, V. & Fäh, D., 2015. A Proposal For Horizontal And Vertical Elastic Design Spectra. Input for the new Swiss code for dams (Technical Report No. SED/BFE/R/01/30072015), Swiss Seismological Service (SED), ETH Zurich. Retrieved from http://seismo.org/Biblio/Reports/ETHZ_BFE_2015.pdf.

Poggi, V., Edwards, B. & Fäh, D., 2011. Derivation of a reference shear-wave velocity model from empirical site amplification, *Bull. seism. Soc. Am.,* **101,** 258–274.

Poggi, V., Fäh, D., Burjanek, J. & Giardini, D., 2012. The use of Rayleigh-wave ellipticity for site-specific hazard assessment and microzonation: application to the city of Lucerne, Switzerland, *Geophys. J. Int.,* **188,** 1154–1172.

Poggi, V., Michel, C., Roten, D., Burjanek, J., Cauzzi, C. & Fäh, D., 2013. Lucerne-Werkhofstresse (SLUW) (Site Characterization Report), Swiss Seismological Service (SED), ETH Zurich, doi:10.12686/sed-stationcharacterizationdb.

Popescu, R. & Prevost, J.H., 1995. Comparison between VELACS numerical 'class A' predictions and centrifuge experimental soil test results, *Soil Dyn. Earthq. Eng.,* **14,** 79–92.

Prevost, J. & Popescu, R., 1996. Constitutive relations for soil materials, *Electron. J. Geotech. Eng.,* **1,** 1–43.

Prevost, J.H., 1985. A simple plasticity theory for frictional cohesionless soils, *Int. J. Soil Dyn. Earthq. Eng.,* **4,** 9–17.

Régnier, J., 2013. Seismic site-response variability: from site-classification to soil non-linear behaviour, *Doctoral thesis*, Earth Sciences. Université Paris-Est. Retrieved from https://tel.archives-ouvertes.fr/tel-00906072.

Régnier, J., 2021. Non-linear soil response at strong motion observation sites with a focus on borehole array, in *Proceedings of the 6th IASPEI/IAEE International Symposium: Effects of Surface Geology on Seismic Motion,* Springer.

Régnier, J. *et al.*, 2018. PRENOLIN: international benchmark on 1D non-linear site-response analysis—validation phase exercise, *Bull. seism. Soc. Am.,* **108,** 876–900.

Régnier, J., Cadet, H., Bonilla, L., Bertrand, E. & Semblat, J.-F., 2013. Assessing non-linear behavior of soils in seismic site response: statistical analysis on KiK-net strong-motion data, *Bull. seism. Soc. Am.,* **103,** 1750–1770.

Resonance & Keller, Lorenz, A.G., 2012. Spektrale Mikrozonierung Luzern für ausgewählte untersuchungsgebiete. (Technischer Bericht), Carouge and Luzern.

Robertson, P., 2009a. Interpretation of cone penetration tests—a unified approach, *Can. Geotech. J.,* **46,** 1337–1355.

Robertson, P., 2009b. Performance based earthquake design using the CPT, in *Proceedings of the International Conference on Performance-Based Design in Earthquake Geotechnical Engineering*.

Robertson, P.K. & Cabal, K.L., 2010. Estimating soil unit weight from CPT, in *Proceedings of the 2nd International Symposium on Cone Penetration Testing (CPT'10),* Huntington Beach, CA, 9–11 May 2010.

Robertson, P.K. & Wride, C.E., 1998. Evaluating cyclic liquefaction potential using the cone penetration test, *Can. Geotech. J.,* **35,** 442–459.

Robertson, P.K., 2012. Interpretation of in-situ tests—some insights, in *J.K. Mitchell Lecture, Proceedings of ISC'4,* Recife, Brazil, September, 2012, pp. 3–24.

Roten, D., 2014. Documentation of tools for analysis of non-linear soil behavior, Swiss Seismological Service (SED), ETH Zurich.

Roten, D., Fäh, D. & Bonilla, L., 2014. Quantification of cyclic mobility parameters in liquefiable soils from inversion of vertical array records, *Bull. seism. Soc. Am.,* **104,** 3115–3138.

Roten, D., Fäh, D. & Laue, J., 2011. Application of a neighbourhood algorithm for parameter identification in a cyclic mobility model, in *4th IASPEI /IAEE International Symposium: Effects of Surface Geology on Seismic Motion,* Santa Barbara, USA, 23–26 August 2011.

Roten, D., Fäh, D., Bonilla, L.F., Alvarez-Rubio, S., Weber, T.M. & Laue, J., 2009. Estimation of non-linear site response in a deep Alpine valley, *Geophys. J. Int.,* **178,** 1597–1613.

Sambridge, M., 1999. Geophysical inversion with a neighbourhood algorithm—I. Searching a parameter space, *Geophys. J. Int.,* **138,** 479–494.

Santucci de Magistris, F., Lanzano, G., Forte, G. & Fabbrocino, G., 2014. A peak acceleration threshold for soil liquefaction: lessons learned from the 2012 Emilia earthquake (Italy), *Nat. Hazards,* **74,** 1069–1094.

Schnabel, P. & Lysmer, J., Bolton Seed., 1972. SHAKE: a Computer Program for Earthquake Response Analysis of Horizontally Layered Sites, a Computer Program Distributed by NISEE/Computer Applications (Report No. EERC 72-12), Earthquake Engineering Research Center, University of California, Berkeley, CA.

Schnellmann, M., Anselmetti, F.S., Giardini, D., McKenzie, J.A. & Ward, S.N., 2002. Prehistoric earthquake history revealed by lacustrine slump deposits, *Geology,* **30,** 1131–1134.

SED., 1983. *National Seismic Networks of Switzerland*, Swiss Seismological Service (SED), ETH Zürich, doi:10.12686/SED/NETWORKS/CH.

SED., 2015. The site characterization database for seismic stations in Switzerland, Swiss Seismological Service (SED), ETH Zürich, doi:10.12686/SED-STATIONCHARACTERIZATIONDB.

SIA261., 2020. Actions on Structures, SIA 261, Swiss Standards, Swiss Society of Engineers and Architects.

Siegenthaler, C., Finger, W. & Kelts, K., 1987. Earthquake and seiche deposits in Lake Lucerne, Switzerland, *Eclogae Geol. Helv.,* **80,** 241–260.

Strasser, M., Anselmetti, F.S., Fäh, D., Giardini, D. & Schnellmann, M., 2006. Magnitudes and source areas of large prehistoric northern Alpine earthquakes revealed by slope failures in lakes, *Geology,* **34,** 1005–1008.

Swisstopo., 2020. Thickness model of unconsolidated deposits. Federal Office of Topography Swisstopo, Retrieved October 1, 2020, from https://s.geo.admin.ch/a05b95a0cf.

Swisstopo., 2023. Geological vector datasets GeoCover (Federal Office of Topography swisstopo), Retrieved March 1, 2024, from https://s.geo.admin.ch/95a803e945.

Towhata, I. & Ishihara, K., 1985. Modeling soil behavior under principal axes rotation, in *Proceedings of the 5th International Conference on Numerical Methods in Geomechanics,* Nagoya, 1–5 April 1985, pp. 523–530.

Trifunac, M.D. & Brady, A.G., 1975. A study on the duration of strong earthquake ground motion, *Bull. seism. Soc. Am.,* **65,** 581–626.

Wathelet, M., Jongmans, D. & Ohrnberger, M., 2004. Surface-wave inversion using a direct search algorithm and its application to ambient vibration measurements, *Near Surf. Geophys.,* **2,** 211–221.

Wiemer, S. *et al.*, 2016. *Seismic Hazard Model* 2015 for Switzerland (SUIhaz2015), Swiss Seismological Service (SED), ETH Zurich. Retrieved from http://www.seismo.ethz.ch/en/knowledge/earthquake-hazard-and-risk/for-professionals/.

Wiemer, S. *et al.*, 2023. Earthquake Risk Model of Switzerland ERM-CH23 (Report No. PMA-FR-0001), Swiss Seismological Service (SED), ETH Zurich. doi:10.12686/a20.

Yang, Z., Elgamal, A. & Parra, E., 2003. Computational model for cyclic mobility and associated shear deformation, *J. Geotech. Geoenviron. Eng.,* **129,** 1119–1127.

Yoshida, N. & Iai, S., 1998. Non-linear site response and its evaluation and prediction, in *Proceedings of the 2nd International Symposium on the Effect of Surface Geology on Seismic Motion,* Yokosuka, Japan, pp. 71–90.

Youd, T. *et al.*, 2001. Liquefaction resistance of soils: summary report from the 1996 NCEER and 1998 NCEER/NSF workshops on evaluation of Liquefaction resistance of soils, *J. Geotech. Geoenviron. Eng.,* **127,** 817–833.

Yu, G., Anderson, J.G. & Siddharthan, R., 1993. On the characteristics of non-linear soil response, *Bull. seism. Soc. Am.,* **83,** 218–244.